Research Experience

List of Publication:

- **Ruchika**, Bhardwaj, N., Saneja, A.* **(2024).** Orally Fast Dissolving α-Lipoic acid Electrospun Nanofibers Mitigates Lipopolysaccharide Induced Inflammation in RAW 264.7 Macrophages. ***International Journal of Biological Macromolecules***, 130623. https://doi.org/10.1016/j.ijbiomac.2024.130623 **(IF:7.7)**

- **Ruchika**, Khan, N., Dogra S. S., Saneja, A.* **(2024).** The Dawning Era of Oral Thin Films for Nutraceutical Delivery: From Laboratory to Clinic. ***Biotechnology Advances***, 108362. https://doi.org/10.1016/j.biotechadv.2024.108362 **(IF:16)**

- **Ruchika**, Bhardwaj, N., Yadav, S.K. and Saneja, A.* **(2024).** Recent advances in 3D bioprinting for cancer research: From precision models to personalized therapies. ***Drug Discovery Today***, 103924. https://doi.org/10.1016/j.drudis.2024.103924 **(IF:6.5)**

- **Ruchika**, Kumari S., Dhiman P., Singh D., Saneja A.* **(2022).** *R*-*α*-Lipoic Acid Conjugated to *D*-*α*-Tocopherol Polyethylene Glycol 1000 Succinate: Synthesis, Characterization, and Effect on Antiseizure Activity. ***Journal of Agricultural and Food Chemistry,*** 70, 25, 7674–7682 https://doi.org/10.1021/acs.jafc.2c01685 **(IF:6.1)**

- **Ruchika**, Sharma A., Saneja A.* **(2022).** Zebrafish as A Powerful Alternative Model Organism for Preclinical Investigation of Nanomedicines, ***Drug Discovery Today***, 27, 5, 1513 - 1522 https://doi.org/10.1016/j.drudis.2022.02.011 **(IF: 6.5)**

- Chhimwal, J., Dhritlahre, R.K., Anand, **Ruchika**, P., Patial, V., Saneja, A. and Padwad, Y.S., **(2023).** Amorphous solid dispersion augments the bioavailability of phloretin and its therapeutic efficacy via targeting mTOR/SREBP-1c axis in NAFLD mice. ***Biomaterials Advances***, 154, 213627. https://doi.org/10.1016/j.bioadv.2023.213627 **(IF: 7.9)**

- Dhritlahre R. K., **Ruchika**, Padwad Y., Saneja A.* **(2021).** Self-emulsifying formulations to augment therapeutic efficacy of nutraceuticals: From concepts to clinic. ***Trends in Food Science & Technology***, 115, 347-365. https://doi.org/10.1016/j.tifs.2021.06.046 **(IF: 15.1)**

- Khan N., **Ruchika**, Dhritlahre R. K., Saneja A.* **(2022).** Recent advances in dual ligand targeted cancer therapy. ***Drug Discovery Today*****,** 27, 2288-2299 https://doi.org/10.1016/j.drudis.2022.04.011 **(IF: 6.5)**

- Khan N., Bhardwaj V.K., **Ruchika**, Purohit R.*, and Saneja A.* **(2023).** Deciphering the interactions of genistein with β-cyclodextrin derivatives through experimental and microsecond timescale umbrella sampling simulations. ***Journal of Molecular Liquids***, 374, 121295 https://doi.org/10.1016/j.molliq.2023.121295. **(IF: 5.3)**

- Sharma, P., **Ruchika,** Dhiman, P., Kumar, R., Saneja, A., & Singh, D. **(2023).** A solid dispersion of Citrus reticulata peel biowaste as an effective antiepileptic: Sustainable approach toward value addition and agro-industrial waste valorisation. ***Journal of Drug Delivery Science and Technology***, 81, 104238 https://doi.org/10.1016/j.jddst.2023.104238 **(IF: 4.5).**

- **Ruchika**, Sharma, K.S., Kumar R., Yadav, S.K. and Saneja, A.* **(2024).** Multifunctional Pterostilbene Nanoemulsion Incorporated Chitosan-Alginate Films for Food Preservation***. Food Packaging and Shelf-Life***. **(IF: 8.5) (Communicated)**

- Kaliya, K., Bhardwaj, N., **Ruchika**, Saneja, A.* **(2024).** Synthesis of a Gemcitabine Prodrug and its Encapsulation into Polymeric Nanoparticles for Improved Therapeutic Efficacy. **(Communicated)**

Book chapters

- **Ruchika**, Saneja A*. (2021). Valorization of Sitosterol from Agricultural Waste as Therapeutic Agent. In: Rana A., Saneja A., Kumar S., Lichtfouse E (eds) Sustainable Agriculture Reviews 56. **Sustainable Agriculture Reviews,** vol 56. Springer, Cham. https://doi.org/10.1007/978-3-030-84405-9_5

- **Ruchika**, Dhritlahre R. K., Saneja A*. (2021) Nano-delivery of Bioactive Constituents from Apple Pomace. In: Rana A., Saneja A., Kumar S., Lichtfouse E (eds) Sustainable Agriculture Reviews 56. **Sustainable Agriculture Reviews**, vol 56. Springer, Cham. https://doi.org/10.1007/978-3-030-84405-9_3

Copy of two research publication is enclosed below

JOURNAL OF AGRICULTURAL AND FOOD CHEMISTRY

pubs.acs.org/JAFC Article

R-α-Lipoic Acid Conjugated to D-α-Tocopherol Polyethylene Glycol 1000 Succinate: Synthesis, Characterization, and Effect on Antiseizure Activity

Ruchika, Savita Kumari, Poonam Dhiman, Damanpreet Singh, and Ankit Saneja*

Cite This: https://doi.org/10.1021/acs.jafc.2c01685 Read Online

ACCESS | Metrics & More | Article Recommendations | Supporting Information

ABSTRACT: α-Lipoic acid (LA), a dithiol micronutrient, acts as a vital cofactor in various cellular catabolic reactions and is also known as a universal antioxidant. The therapeutic efficacy of LA is compromised by a poor aqueous solubility as well as a short half-life. In the present study, LA was conjugated to D-α-tocopherol polyethylene glycol succinate (TPGS) using carbodiimideacid−alcohol coupling reaction. The synthesized conjugate (TPGS-LA) was characterized using ^{1}H and ^{13}C nuclear magnetic resonance (NMR), Fourier transform infrared spectroscopy (FT-IR), UV−vis spectroscopy, and matrix-assisted laser desorption/ionization time-of-flight mass spectrometry (MALDI-TOF MS). The TPGS-LA conjugate was demonstrated to be biocompatible and to have better anticonvulsion activity as compared to native LA in pentylenetetrazol (PTZ)-induced convulsions in zebrafish. Moreover, zebrafish larvae pretreated with TPGS-LA conjugate demonstrated a significant ($p < 0.05$) reduction of protein carbonylation levels and downregulation of *c-fos* expression during seizures as compared to native LA. Conclusively, the present findings demonstrate that the TPGS-LA conjugate can be a promising approach for the delivery of LA.

KEYWORDS: *lipoic acid, tocopherol poly(ethylene glycol) 1000 succinate, zebrafish, epilepsy, anticonvulsion activity*

INTRODUCTION

α-Lipoic acid (LA, 6,8-dithiooctanoic acid), an organosulfur compound belonging to the B-vitamins group, has a strong antioxidant potential.[1] Indeed, it is also recognized as a "universal antioxidant" reasoned to scavenge free radical species in direct (suppress and scavenge radical species directly) and indirect (initiating the transcription of antioxidant enzymes via the nucleus) ways. Moreover, it is effective in the prevention or treatment of various diseases such as liver,[2] cardiovascular,[3] diabetes,[4] and Alzheimer's[5] diseases. A recent study found that LA dramatically reduced the occurrence of epileptic seizures and alleviated the behavioral dysfunction in rats induced by pentetrazol via an Nrf2 pathway.[6] It is also reported that a deficiency of LA inside the body may lead to early infantile epileptic encephalopathy.[7] Despite its tremendous therapeutic potential, LA is associated with poor aqueous solubility, short half-life (~30 min), and poor bioavailability (about 30%) which ultimately limits its therapeutic efficacy.[8]

To overcome these limitations, much attention has been given to the development of LA delivery systems such as the self-emulsifying delivery system (SEDDS),[9] nanoemulsions,[10] polymeric nanoparticles,[11] lipid nanoparticles,[12] etc. However, one of the most promising approaches to tackle these challenges is to explore polymer conjugates of these therapeutic agents which also have the ability to self-assemble into nanostructures. In this regard, a nonionic, amphiphilic self-assembling tocopherol polyethylene glycol succinate (TPGS) polymer is gaining tremendous attention for the delivery of therapeutic agents because of its GRAS (generally recognized as safe) status and its use as an absorption enhancer and stabilizer in various formulations. The conjugation of TPGS with several drugs such as paclitaxel,[13] doxorubicin,[14] cantharidin,[15] and gemcitabine[16] has demonstrated better therapeutic efficacy as compared to their native counterparts. More interestingly, the surface modifications of nanoformulations with TPGS and its derivatives have been demonstrated to overcome biological barriers including the blood−brain barrier (BBB) by enhancing uptake of these formulations.[17] On the other side, zebrafish experimental models are now receiving tremendous attention to explore the pathophysiology and pharmacology of neurological diseases such as epilepsy,[18] Parkinson's disease,[19] and motor neuron diseases.[20]

Therefore, considering these aspects, in the present investigation, we have conjugated LA with TPGS via an ester bond. The characterization of the synthesized conjugate was executed using different analytical techniques such as ^{1}H NMR, ^{13}C NMR, and FT-IR. Molecular weights of TPGS and the synthesized TPGS-LA conjugate have been analyzed using matrix-assisted laser desorption/ionization time-of-flight mass spectrometry (MALDI-TOF MS) . The biocompatibility of the synthesized conjugate has been assessed using zebrafish embryos/larvae. The antiepileptic evaluation of the TPGS-LA conjugate was performed using pentylenetetrazol (PTZ)-

Received: March 9, 2022
Revised: May 25, 2022
Accepted: June 3, 2022

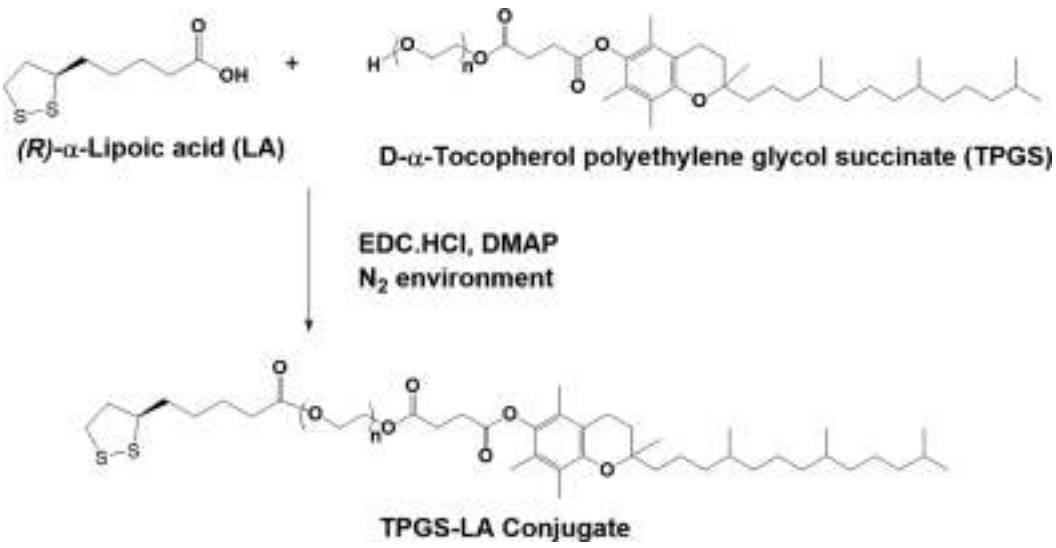

Figure 1. Synthetic scheme for D-α-tocopherol polyethylene glycol succinate 1000 (TPGS)-lipoic acid (TPGS-LA) conjugate. EDC·HCl: 1-Ethyl *N*-3-(3-(dimethylamino)propyl)) carbodiimide hydrochloric acid. DMAP: 4-(Dimethylamino) pyridine.

induced convulsions in zebrafish larvae. Finally, the effect of the LA and TPGS-LA conjugate treatment on the protein carbonylation and expression of *c-fos*, a transsynaptic marker of neuronal activity in the zebrafish larval brain, was assessed.

MATERIALS AND METHODS

Materials. D-α-Tocopherol polyethylene glycol 1000 succinate (TPGS), pentylenetetrazol (PTZ), anhydrous dichloromethane (DCM), 4-(dimethylamino) pyridine (DMAP), a Pur-A-Lyzer dialysis kit (MWCO 1 kDa), and TRIZOL reagent were purchased from Sigma-Aldrich. (*R*)-α-Lipoic acid (LA) was purchased from Tokyo Chemical Industry (TCI). 1-ethyl *N*-3-(3-(dimethylamino)propyl) carbodiimide hydrochloric acid (EDC·HCl) was procured from HiMedia Laboratories. A Verso cDNA synthesis kit and GoTaq qPCR Master Mix were procured from Thermo Fisher Scientific and Promega, respectively. All other solvents and reagents used were of analytical grade.

Synthesis of TPGS-(R)-α-Lipoic Acid Conjugate (TPGS-LA). TPGS-Lipoic acid (TPGS-LA) conjugate was synthesized via a single-step carbodiimide acid−alcohol coupling reaction by using EDC·HCl as a coupling agent and DMAP as a base[14,21] (Figure 1). In a 50 mL round-bottom flask, LA (3 equiv), EDC·HCl (3 equiv), and DMAP (0.1 equiv) were dissolved in 10 mL of anhydrous dichloromethane (CH_2Cl_2) for 20 min under a N_2 environment in an ice bath. To the above reaction mixture, TPGS (500 mg, 0.33 mM, 1 equiv) in 5 mL of dichloromethane was added, and the reaction was continued with stirring for 36 h under a N_2 environment at room temperature (RT). The resultant product was dried under reduced pressure, dissolved in ethanol, and dialyzed (via a Pur-A-Lyzer dialysis kit, MWCO 1 kDa) in two steps for 72 h, first against 70% ethanol for 24 h and then against deionized water for 48 h to remove unreacted LA and side products. The purified product was lyophilized (Labconco FreeZone freeze-dryer) and stored at −20 °C for further use.

Characterization of TPGS-LA Conjugate. The conjugation of LA with TPGS was analyzed using NMR, FT-IR, and MALDI. ^{1}H NMR (600 MHz) and ^{13}C NMR (151 MHz) spectra were recorded for LA, TPGS, and TPGS-LA conjugate by an NMR spectrometer (AV-600, Bruker) using $CDCl_3$ as the solvent. The FT-IR spectra were recorded using a PerkinElmer FT-IR spectrometer in chloroform over the range 4000−500 cm^{-1}. The mass spectrum of TPGS and TPGS-LA was obtained by MALDI-TOF (Bruker Ultraflex TOF/TOF), ranging from 1000 to 2400 Da. UV spectra of synthesized TPGS-LA conjugate were also analyzed using a GENESYS 180 UV−vis spectrophotometer.

Zebrafish Husbandry and Embryo Culture. A wild type zebrafish (*Danio rerio*) strain was reared in a standalone system (Tecniplast, Buguggiate, Varese, Italy) maintaining the standard aquatic environment, proper aeration, and four-stage filtration system. Housing tanks were maintained at controlled aquatic conditions of 7.0−7.5, 26−28 °C, and 400−600 μS values for the pH, temperature, and conductivity of the system water, respectively. Zebrafish were fed a live diet (*Artemia*, Inve Aquaculture, Inc., Salt Lake City, UT) two times a day with a 14 h light and 10 h dark cycle. For breeding purposes, special breeding tanks were placed at a 2:1 female to male ratio, and thereafter, healthy eggs were collected in a glass Petri dish and cleaned thrice with system water. After cleaning, eggs were raised in a biological oxygen demand (BOD) incubator maintained at 28.5 ± 0.5 °C with the water changed daily. The experimental protocol was approved by the Institutional (CSIR-IHBT) Animal Ethics Committee (IAEC).

Evaluation of Biocompatibility of TPGS-LA on Zebrafish. The biocompatibility of synthesized TPGS-LA conjugate was investigated by analyzing the complete embryonal development of zebrafish embryos up to 120 h postfertilization (hpf).[22] In brief, 4 hpf embryos were collected and cleaned thrice with system water carefully to avoid any contamination. Embryos were randomly divided into four groups [Naïve vehicle (NV) and three groups of TPGS-LA conjugate] with 20 embryos in each group. Naïve group embryos were reared in 2 mL of system water in a 24-well plate with 3 embryos in each well, whereas treatment group embryos were cultured in system water with concentrations of 5, 10, and 20 μM TPGS-LA conjugate (equivalent to LA) in the BOD incubator maintained at 28.5 ± 0.5 °C. The solution was changed thrice in 24 h, and all developmental stages were observed under a Nikon stereomicroscope (SMZ 800N, Nikon, Tokyo, Japan). Numbers of surviving and hatching embryos were observed carefully, and survival and hatching rate percentages were calculated using the following equations:

$$\text{survival rate of embryos (\%)} = \frac{\text{number of healthy embryos}}{\text{total number of embryos}} \times 100$$

$$\text{hatching rate of embryos (\%)} = \frac{\text{number of hatched embryos}}{\text{total number of embryos}} \times 100$$

Evaluation of Seizure Latency and Locomotor Activity Tests on PTZ-Induced Seizures. The PTZ drug, a common chemo-convulsant, acts as an antagonist to the γ-aminobutyric acid (GABA) receptor and induces seizures. PTZ-induced seizures in the zebrafish larvae manifest three different stages, i.e., stage I, hyperactivity stage, characterized by an increase in speed and abnormal swimming

https://doi.org/10.1021/acs.jafc.2c01685
J. Agric. Food Chem. XXXX, XXX, XXX−XXX

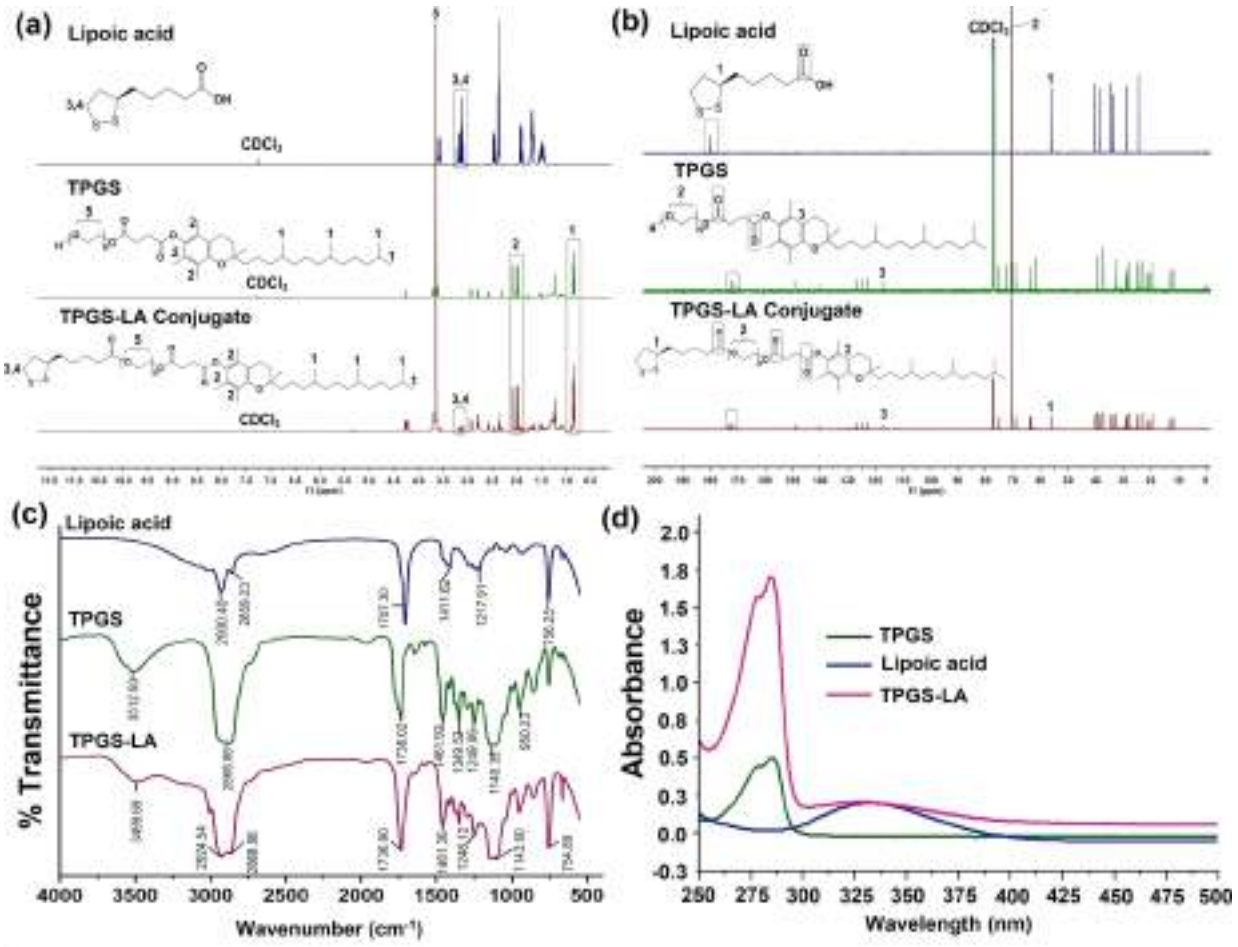

Figure 2. (a) ^{1}H (600 MHz) and (b) ^{13}C NMR (151 MHz) spectra of native lipoic acid (LA), TPGS, and TPGS-LA conjugate in deuterated chloroform ($CDCl_3$). The NMR spectrum of TPGS-LA conjugate demonstrated peaks of both TPGS and LA. The peak in the ^{13}C NMR at δ 180 ppm (due to the carboxylic group of lipoic acid) was shifted upfield to δ 173 ppm in TPGS-LA conjugate due to ester bond formation. (c) Stacked Fourier transform-infrared (FT-IR) spectra of LA, TPGS, and TPGS-LA with a scanning range from 4000 to 500 cm^{-1}. (d) UV−vis spectra of LA, TPGS, and TPGS-LA conjugate.

pattern; stage II, whirlpool stage exhibiting circular whirlpool-like movements; and stage III, clonus-like seizure stage with strong body twitching movements resulting in a sloping position accompanied by complete loss of posture.[22] Concisely, 7 dpf larvae were randomly divided into four groups, LA1, LA5, LA10, and TPGS-LA, with 10 larvae in each group, and were incubated for 1 h in 1, 5, and 10 μM concentrations of LA and a 5 μM concentration (equivalent to LA) of TPGS-LA conjugate, respectively (dpf, days postfertilization). After incubation, each larva was gently transferred to the well [3.5 cm (diameter), 2 cm (depth)] containing 3.5 mL of 8 mM PTZ solution maintained at 28 ± 0.5 °C, and latency to first clonus seizures (stage III) was noted with a fixed upper cut-off timing of 15 min. Furthermore, distance traveled and mean velocity as an index of hyperactive response were recorded for an initial 5 min. For recording and eliminating human error, a camera (c922 Pro Stream, Logitech Asia Pacific Ltd., Hong Kong) connected with a video tracking system (SMART V.3.0.Panlab Barcelona) was used. Naïve vehicle (NV) and the PTZ-treated group were also recorded separately.

Real-Time Quantitative PCR to Assess the Modulation of the mRNA Levels of *c-fos*. c-*fos* gene expression was analyzed in treated as well as nontreated 7 dpf larva as reported earlier.[22] In brief, 7 dpf zebrafish larvae were randomly categorized in four groups, namely, naïve control (NV; with system water), vehicle control (PTZ), lipoic acid (LA10; 10 μM), and TPGS-LA conjugate (TPGS-LA; 5 μM equivalent to LA). Every group had three independent sets of 20 larvae each.[23] After incubation, all groups were exposed to 8 mM PTZ solution for 15 min separately, except the naïve group. The exposed larvae were sacrificed, and RNA isolation was performed by using TRIZOL reagent (Sigma-Aldrich). The isolated RNA sample was further processed into cDNA using the Verso cDNA synthesis kit (Thermo Fisher Scientific) as per the instructions provided by the manufacturer. Further, the quantitative real-time polymerase chain reaction (AriaMx Real-Time PCR, Agilent Technologies) was carried out by using GoTaq qPCR Master Mix (Promega). Primers were designed via Primer3 Input (v.0.4.0) software and have sequences *eef1a1b*, [F, TATCTCAAAGAACGGGCAAA; R, TTCACAATC-TCCTCATAGCG]; and *c-fos*, [F, TTACCGGTGCTAGATTTGTT; R, ATTCACACGTTCAGAAATCC]. *eef1a1b* was used as an internal control for qRT PCR analysis. The 2^ddCT method was used to analyze the gene expression, and each value was expressed relative to the naïve control.

Protein Carbonylation Assay to Assess the Modulation of Oxidative Stress Levels. The leftover supernatant following the RNA isolation was used for protein isolation. The DNA was first isolated from the leftover solution to avoid nucleic acid contamination as described earlier.[24] Further, chilled isopropanol was added in the supernatant collected after DNA isolation for precipitation, followed by 10 min of incubation and centrifugation at 12 000*g* for 5 min at 4 °C. The obtained protein pellet was washed thrice with 0.3 M guanidine hydrochloride solution (in 95% ethanol) and finally with absolute ethanol. The protein pellet was air-dried, resuspended in rehydration buffer, and stored at −20 °C for further use. Protein concentration was analyzed by Bradford assay.[25] For the determination of levels of protein carbonylation due to oxidative stress in

https://doi.org/10.1021/acs.jafc.2c01685
J. Agric. Food Chem. XXXX, XXX, XXX−XXX

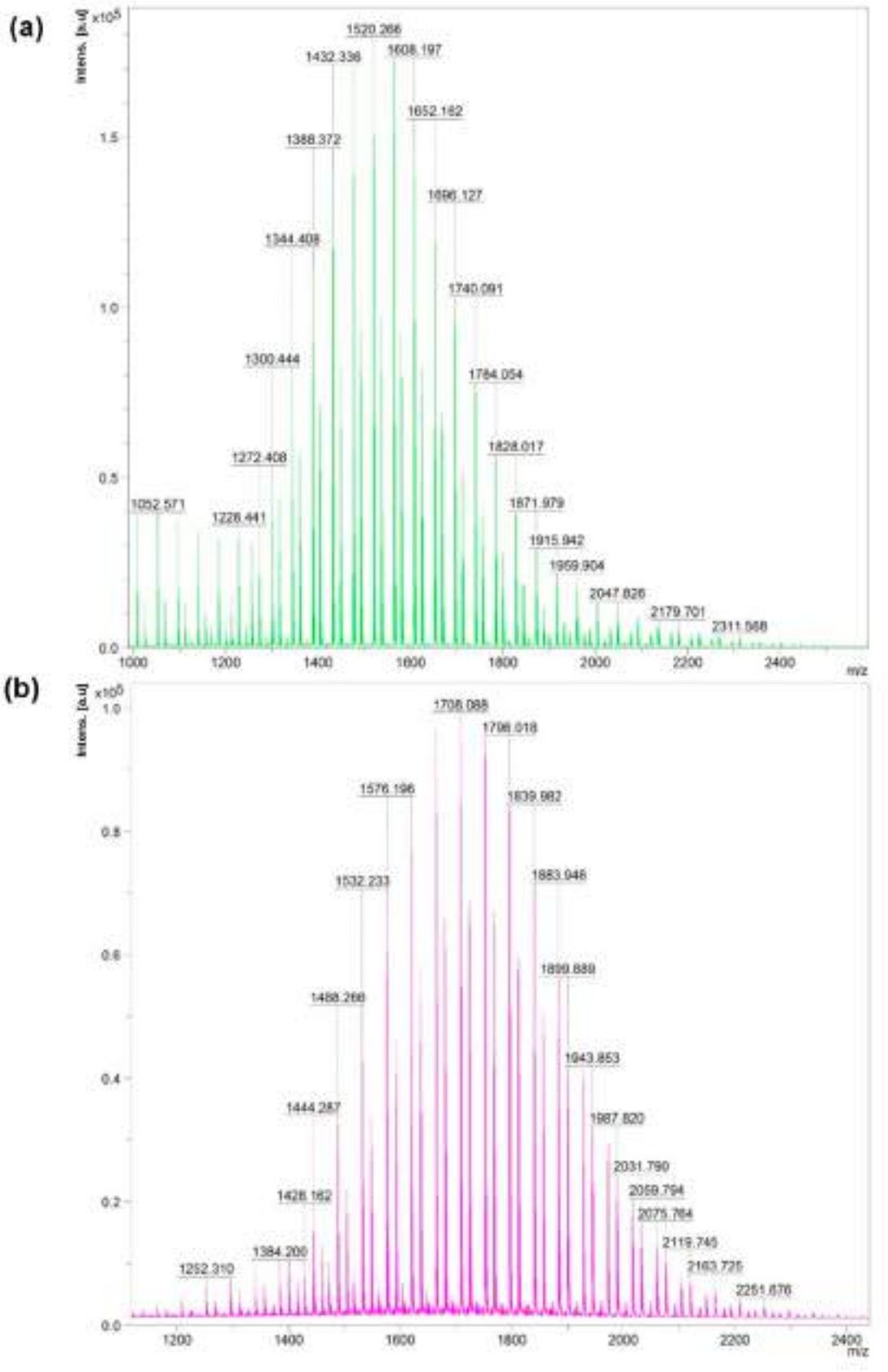

Figure 3. MALDI-TOF spectra of (a) TPGS and (b) TPGS-LA conjugate with a scanning range from 1000 to 2400 Da. Each peak of TPGS-LA conjugate spectra shifted by a common mass factor of 188 Da which corresponds to the mass of one LA molecule covalently conjugated with one molecule of TPGS.

https://doi.org/10.1021/acs.jafc.2c01685
J. Agric. Food Chem. XXXX, XXX, XXX−XXX

larvae, the most frequently used protein carbonylation spectrophotometric assay was performed. Briefly, an equal volume of 2,4-dinitrophenylhydrazine (DNPH) (10 mM in 0.5 M H_3PO_4) and protein with an equivalent concentration from all samples were mixed and incubated for 15 min in the dark. Further, 50% w/v trichloroacetic acid solution was added to the mixture for the precipitation of DNPH adduct, and the mixture was incubated at 20 °C for 15 min. The resultant solution was centrifuged, and the DNPH adduct pellet was collected, washed thrice with a mixture of binary solvents [ethanol/ethyl acetate (1:1 v/v)], and solubilized in 6 M guanidine hydrochloride. The absorbance was recorded at 370 nm, and quantification was performed with a molar coefficient of 22 000 M^{-1} cm^{-1}.

STATISTICS

The results of latency to clonus-like seizures, total distance traveled, mean speed, protein carbonylation content, and relative mRNA levels were represented as mean ± standard error. The level of significance at $p < 0.05$ among different groups was analyzed by a one-way analysis of variance followed by Tukey's post hoc test with SigmaStat statistical software.

RESULTS AND DISCUSSION

Synthesis and Characterization of TPGS-LA Conjugate. In this study, we have explored the polymer drug conjugation approach to augment the therapeutic efficacy of α-lipoic acid. TPGS-LA conjugate was synthesized via esterification between the carboxylic acid group of LA with the hydroxyl group of TPGS. Excessive LA was used in order to achieve a complete reaction as it is easier to separate the low-molecular-weight LA from the large molecular TPGS-LA conjugate. The synthesized TPGS-LA conjugate was confirmed by ^1H and ^{13}C NMR spectroscopy (Figure 2a,b). The ^1H NMR spectrum of TPGS demonstrated characteristic peaks of methylene protons in vitamin E at δ 0.86 ppm and CH_2—CH_2—O— (PEG chain) protons at δ 3.6 ppm[13,26] (Figure 2a). Similar peaks were observed in the ^1H NMR spectrum of TPGS-LA conjugate along with peaks corresponding to LA at δ 3.11−3.18 ppm, thus confirming the successful reaction between TPGS and LA.[27] Further, ^{13}C NMR of TPGS-LA conjugate shows the peaks of both LA and TPGS (Figure 2b). The spectrum of TPGS demonstrated peaks at δ 171 and δ 172 ppm corresponding to its two carbonyl (—C═O) groups. The peak in the ^{13}C NMR results at δ 180 ppm (because of the carboxylic group of LA) was shifted upfield to δ 173 ppm in TPGS-LA conjugate due to ester bond formation, and a total of three peaks at the δ 171, δ 172, and δ 173 ppm region were observed, representing three carbonyl groups (two of TPGS and one of LA).[28] Moreover, from the integration in ^1H NMR peaks, it was concluded that approximately 95% of LA is conjugated with TPGS.

The FT-IR spectra of native TPGS shows a characteristic band at 1738.02 cm^{-1} which attributes to the carbonyl group (C═O) present in the TPGS.[16] While comparing FT-IR spectra of LA with those of TPGS-LA, a shifting and strong absorption of the carbonyl band from 1707.30 to 1736.90 cm^{-1} was observed, confirming the replacement of the carboxyl group with the ester moiety, which thus provides evidence of ester bond formation between TPGS and LA.[29] Additionally, peaks at 1143.60 and 2924.54 cm^{-1} correspond to —COO— and —CH_2 group stretching in TPGS, respectively (Figure 2c). UV−vis spectra of conjugate were also recorded which reveal the appearance of both of the peaks corresponding to the λ_{max} of both TPGS (λ_{max} 280 nm) as well as LA (λ_{max} 332 nm) which is usually observed in polymer drug conjugates[30] (Figure 2d).

The conjugation of LA with TPGS was also confirmed using MALDI-TOF MS (Figure 3). The MALDI spectra of TPGS and TPGS-LA conjugate both demonstrated a peak variation of 44 Da between each peak because of CH_2CH_2O repeating monomeric units of PEG. LA has a mass of 206.32 Da, and its covalent linkage with TPGS should demonstrate a mass increase of about 188 Da in its oligomeric structure as compared to TPGS, demonstrating the successful conjugation of LA with TPGS (see Table S1). For instance, the peak of TPGS at 1520 has been shifted to 1708, which is equivalent to one LA molecule.

Biocompatibility of TPGS-LA Conjugate on Zebrafish. The zebrafish is now a renowned model for assessing the biocompatibility of therapeutic agents because of its rapid and *ex utero* development which is ideally suited for the screening of potent molecules.[31] Therefore, the biocompatibility of synthesized TPGS-LA conjugate was assessed in zebrafish embryos, and any maltransformations/lethality was observed until 120 hpf. The end point includes coagulation of embryos; loss of heartbeat; delayed hatching; deformation in the tail, eyes, and head; and reduced pigmentation.[32] One distinctive aspect of zebrafish development is their sensitivity toward administered solutions in terms of timing and extent of hatching (which occurs around 2−3 dpf). Based on these aspects, survival, hatching rate, and overall embryonic development of larvae were monitored[33] (see the Supporting Information, Figures S1 and S2). Our results demonstrated that TPGS-LA conjugate imposed negligible variations in the morphology as well as the overall activity of larvae up to a 20 μM concentration (equivalent to LA; Figure 4).

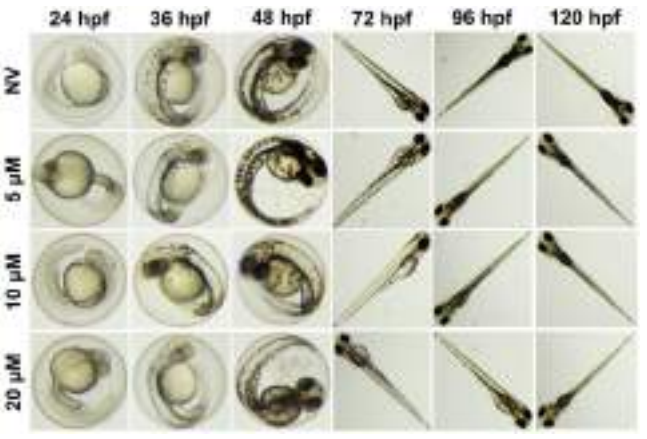

Figure 4. Photographic representation of the embryonic development of zebrafish upon treatments with different concentrations of TPGS-LA conjugate (5, 10, and 20 μM equivalent to LA) in system water over a period from 24 to 120 hpf.

Effects of TPGS-LA Conjugate on Behavioral Seizure Response Post-PTZ. PTZ is a chemical agent that causes seizures in animals by blocking the functioning of chloride channels via binding to the $GABA_A$ receptor.[34] PTZ is considered to be a potent chemoconvulsant commonly used in the development of experimental seizure models.[35] Zebrafish larvae also behave identical to rodents when exposed to PTZ and exhibit concentration-dependent convulsing activity.[36] Here, we have used an 8 mM concentration of PTZ

https://doi.org/10.1021/acs.jafc.2c01685
J. Agric. Food Chem. XXXX, XXX, XXX−XXX

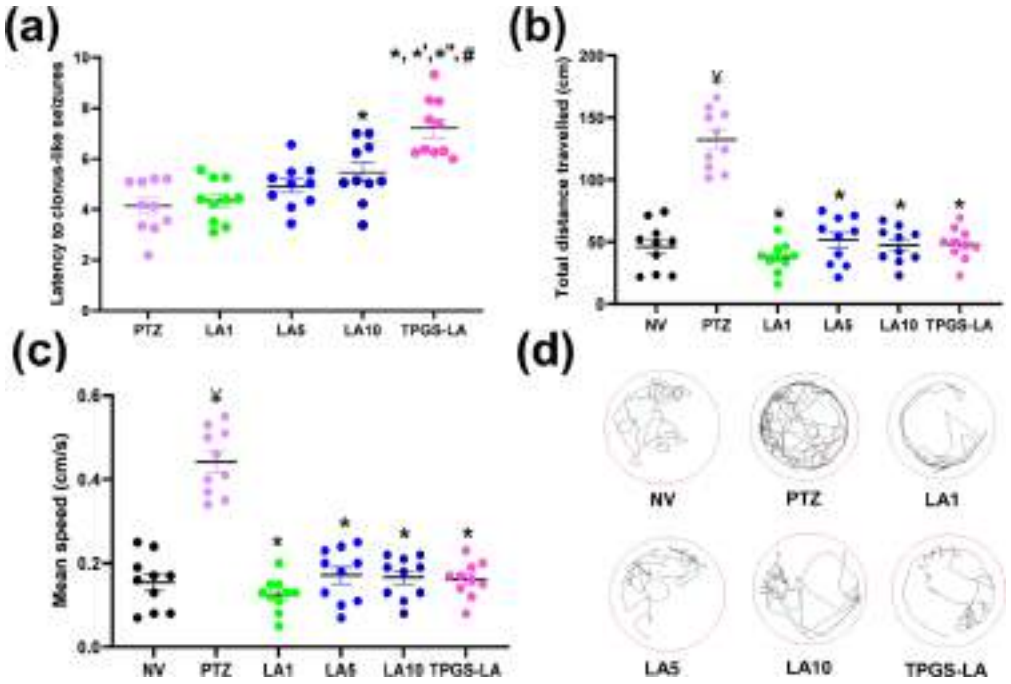

Figure 5. Effect of LA and TPGS-LA conjugate on (a) latency to clonus-like seizure and PTZ- induced hyperactivity as (b) total distance traveled in cm and (c) mean speed in cm/s. (d) Movement track of 7 dpf larva during PTZ exposure for 5 min. $^{¥}p < 0.05$ as compared to NV, $^{*}p < 0.05$ as compared to PTZ, $^{*'}p < 0.05$ as compared to LA1, $^{*''}p < 0.05$ as compared LA5, and $^{\#}p < 0.05$ as compared LA10. NV: 7 dpf larvae incubated in system water, not exposed to PTZ. PTZ: system-water-incubated 7 dpf larva exposed to PTZ (8 mM). LA1: lipoic acid (1 μM)-incubated larva exposed to PTZ. LA5: lipoic acid (5 μM)-incubated larva exposed to PTZ. LA10: lipoic acid (10 μM)-incubated larva exposed to PTZ. TPGS-LA: TPGS-LA (equivalent to 5 μM lipoic acid)-incubated larva exposed to PTZ.

which potentially induced a hyperactive response within the first few minutes of exposure followed by severe seizures to loss of posture as time passed. It has been established that the pretreatment of any antiepileptic compound or entity decreases the PTZ-induced hyperactive response and increases the time for the arrival of clonus-like seizures in the respective animal model.[37]

As seizures or convulsions are the most prominent and distinct symptom of epilepsy, latency in the arrival of clonus-like seizures was recorded to evaluate the pretreatment antiepileptic potential of synthesized TPGS-LA conjugate. Preincubated TPGS-LA conjugate (5 μM equivalent to LA) larvae and LA10 (10 μM) exhibited an increment in latency to PTZ-induced convulsions in comparison to PTZ and other LA groups (LA1 and LA5; Figure 5a). There was a significant ($p < 0.05$) increase in timing of clonus-like seizures in TPGS-LA conjugate (7.5 min) as compared to the PTZ group (4.1 min) and LA groups (LA1, 4.5 min; LA5, 4.9 min; and LA10, 5.53 min) whereas differences among LA1 and LA5 groups in comparison to the PTZ group were observed to be insignificant.

Here, PTZ potentially induces a hyperactive response in larvae exposed with PTZ as compared to the naïve control as there was a significant ($p < 0.05$) difference in total distance traveled in the PTZ group in comparison to the naïve control (Figure 5b). However, preincubation with TPGS-LA at 5 μM (equivalent to LA) and LA at 1, 5, and 10 μM demonstrated a significant decrease in total distance traveled in contrast to the PTZ group ($p < 0.05$).

A similar trend was observed in the swimming pattern and speed in all groups. The PTZ group showed a marked increase in the mean speed of larvae at a significance level of $p < 0.05$ as compared to the naïve group. A significant ($p < 0.05$) decrease in speed was observed in all treatment groups (LA1, LA5, LA10, and TPGS-LA) in contrast to the PTZ group (Figure 5c).

Increased speed and locomotor activity are the first sign of seizurelike behavior in epileptic zebrafish. Thus, suppression and regulation of these parameters can indicate the antiepileptic activity of the compound.[6] Here, we observed a similar pattern, as PTZ-treated larvae demonstrated increased distance traveled and mean speed, whereas the treatment group suppresses all of these behaviors. All of these findings align with previously reported findings that any antiepileptic entity potentially improves and regulate seizure-associated indicators and also delays the onset of seizures in *in vivo* models and also in humans.[22,38,39] Consequently, the results of the current study suggest that TPGS-LA conjugate significantly decreased the hyperactive response (total distance traveled and mean speed) and also exhibited increased latency to clonus-like seizures at a 5 μM concentration in comparison to both PTZ and LA (1, 5, and 10 μM concentrations) groups.

Effect of TPGS-LA Conjugate on Protein Carbonylation. Epilepsy is a dynamic process of frequent neuronal deaths which may be due to several factors. One of the most common factors is oxidative stress as the brain is an organ that is highly susceptible to oxidative stress, and high levels of intracellular calcium during seizures can induce free radical species.[39] Oxidative stress results in oxidation of proteins, lipids, and nucleotides which has a great impact on pathophysiological conditions. Protein carbonylation is considered as the hallmark of oxidative stress in the brain. Thus, the level of protein carbonylation was determined by using a DNPH-based protein carbonylation assay. This involves the formation of stable dinitrophenyl (DNP) hydrazone after the reaction with carbonyl group of proteins.[40] A significant

https://doi.org/10.1021/acs.jafc.2c01685
J. Agric. Food Chem. XXXX, XXX, XXX−XXX

increase ($p < 0.05$) in carbonylation of protein was observed in the PTZ-treated group of larvae in comparison to the naïve group. TPGS-LA-treated groups exhibited a marked decrease in protein carbonylation levels in comparison to PTZ (Figure 6a). However, no significant difference in protein carbonylation was observed between PTZ and LA10 groups. These results indicated that TPGS-LA at a 5 μM concentration significantly reduces the formation of carbonylated protein via reducing oxidative stress in comparison to the native LA at 10 μM.

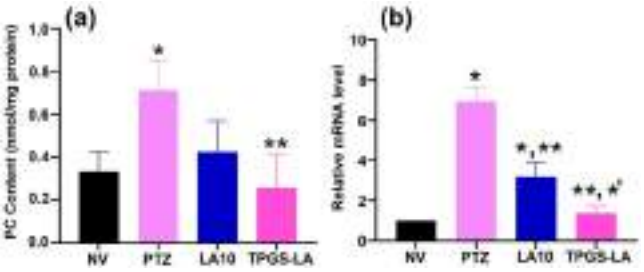

Figure 6. Effect of LA and TPGS-LA on (a) protein carbonylation levels in larvae exposed to PTZ and (b) *c-fos* expression of larvae exposed to PTZ. *$p < 0.05$ as compared to NV, **$p < 0.05$ as compared to PTZ, and *'$p < 0.05$ as compared to LA10. NV: 7 dpf larvae incubated in system water, not exposed to PTZ. PTZ: system-water-incubated 7 dpf larva exposed to PTZ (8 mM). LA10: lipoic acid (10 μM)-incubated larva exposed to PTZ. TPGS-LA: TPGS-LA conjugate (5 μM)-incubated larva exposed to PTZ.

Effect of TPGS-LA Conjugate on the mRNA Expression of *c-fos*. *c-fos* is considerably used to detect aberrant neuronal activation and is proposed to be positively related with level of convulsions as it is upregulated in the case of seizures, inflammation, and injury.[37,41] It plays a significant role in various neuronal physiological processes and is also related to neuronal malfunctioning and cell death in excitotoxicity conditions.[42] To assess the effect of pretreatment of TPGS-LA conjugate (5 μM equivalent to LA) and LA (10 μM) on *c-fos* expression, *c-fos* mRNA expression was assessed via quantitative PCR. Our results revealed that PTZ significantly upregulated *c-fos* expression as compared to the naive control, whereas TPGS-LA conjugate significantly downregulated the *c-fos* expression in comparison to both PTZ and LA groups (Figure 6b).

Our results are in corroboration with the earlier finding on PTZ-induced upregulation of *c-fos* expression in 7 dpf zebrafish larvae and also in rodent models.[38,43] It is well-reported that PTZ exposure increases *c-fos* expression by several fold in different regions of the zebrafish larval brain, and the antiseizure entity reduces its expression.[22,38,44] Altogether, our results demonstrated an ameliorated effect of TPGS-LA conjugate as compared to native LA in terms of latency in seizures, reduced hyperactivity, and downregulation of *c-fos* gene expression which are the markers of epilepsy, thus reflecting an enhanced protective effect of TPGS-LA as compared to native LA in PTZ-induced convulsions.

In this investigation, we have synthesized and characterized TPGS-LA conjugate via the conjugation of the LA carboxylic group with the hydroxyl group of TPGS. Further, the synthesized TPGS-LA conjugate exhibited an enhanced antiseizure activity in comparison to LA via increasing latency in clonus like seizures, a decreased hyperactive response of zebrafish larvae, and a reduction in oxidative stress. Moreover, conjugate also potentially downregulates *c-fos* expression (a marker of neuronal activity) in PTZ-induced convulsion in larvae. In summary, our findings concluded that TPGS-Lipoic acid conjugate can be a promising approach for ameliorating the therapeutic efficacy of lipoic acid.

■ ASSOCIATED CONTENT

Supporting Information

The Supporting Information is available free of charge at https://pubs.acs.org/doi/10.1021/acs.jafc.2c01685.

Details of the experimental molecular weight of TPGS-LA conjugate recorded by MALDI-TOF and readouts of survival and hatching rates of the biocompatibility experiment after the exposure of TPGS-LA conjugate over a period of 5 days (PDF)

■ AUTHOR INFORMATION

Corresponding Author

Ankit Saneja − *Formulation Laboratory, Dietetics and Nutrition Technology Division, CSIR−Institute of Himalayan Bioresource Technology, Palampur 176061 Himachal Pradesh, India; Academy of Scientific and Innovative Research (AcSIR), Ghaziabad 201002 Uttar Pradesh, India;* orcid.org/0000-0002-2423-4704; Phone: 91-1894-233339; Email: ankitsaneja@ihbt.res.in; Fax: +91-1894-230433

Authors

Ruchika − *Formulation Laboratory, Dietetics and Nutrition Technology Division, CSIR−Institute of Himalayan Bioresource Technology, Palampur 176061 Himachal Pradesh, India; Academy of Scientific and Innovative Research (AcSIR), Ghaziabad 201002 Uttar Pradesh, India*

Savita Kumari − *Pharmacology and Toxicology Laboratory, Dietetics and Nutrition Technology Division, CSIR−Institute of Himalayan Bioresource Technology, Palampur 176061 Himachal Pradesh, India; Academy of Scientific and Innovative Research (AcSIR), Ghaziabad 201002 Uttar Pradesh, India*

Poonam Dhiman − *Pharmacology and Toxicology Laboratory, Dietetics and Nutrition Technology Division, CSIR−Institute of Himalayan Bioresource Technology, Palampur 176061 Himachal Pradesh, India; Academy of Scientific and Innovative Research (AcSIR), Ghaziabad 201002 Uttar Pradesh, India*

Damanpreet Singh − *Pharmacology and Toxicology Laboratory, Dietetics and Nutrition Technology Division, CSIR−Institute of Himalayan Bioresource Technology, Palampur 176061 Himachal Pradesh, India; Academy of Scientific and Innovative Research (AcSIR), Ghaziabad 201002 Uttar Pradesh, India*

Complete contact information is available at: https://pubs.acs.org/10.1021/acs.jafc.2c01685

Funding

The authors acknowledge financial assistance from Science and Engineering Research Board (SERB), New Delhi, for the GAP-270 project (File SRG/2020/000141) and Council of Scientific and Industrial Research (CSIR), New Delhi for MLP-204 project.

Notes

The authors declare no competing financial interest.

■ ACKNOWLEDGMENTS

The authors are grateful to the Director, CSIR-Institute of Himalayan Bioresource Technology, for his continuous support and encouragement. R. acknowledges Council of Scientific and Industrial Research (CSIR), New Delhi, for providing a fellowship (File 31/054(0163)/2020-EMR-I). P.D. is grateful to the CSIR, New Delhi, India, for granting a Junior Research Fellowship (File 31/054(0158)/2020-EMR-I). The Authors acknowledge the central instrumentation facility at CSIR—Indian Institute of Integrative Medicine (IIIM) Jammu for carrying out FT-IR analyses. This Article is institutional communication 4953.

■ ABBREVIATIONS USED

LA, lipoic acid; TPGS, D-α-tocopherol poly(ethylene glycol) 1000 succinate; PTZ, pentylenetetrazol

■ REFERENCES

(1) Salehi, B.; Berkay Yılmaz, Y.; Antika, G.; Boyunegmez Tumer, T.; Fawzi Mahomoodally, M.; Lobine, D.; Akram, M.; Riaz, M.; Capanoglu, E.; Sharopov, F. Insights on the use of α-lipoic acid for therapeutic purposes. *Biomolecules* **2019**, *9* (8), 356.

(2) Yang, Y.; Li, W.; Liu, Y.; Sun, Y.; Li, Y.; Yao, Q.; Li, J.; Zhang, Q.; Gao, Y.; Gao, L. Alpha-lipoic acid improves high-fat diet-induced hepatic steatosis by modulating the transcription factors SREBP-1, FoxO1 and Nrf2 via the SIRT1/LKB1/AMPK pathway. *Journal of nutritional biochemistry* **2014**, *25* (11), 1207−1217.

(3) Jamshidi, K.; Abdollahzad, H.; Nachvak, M.; Rezaei, M.; Golpayegani, M. R.; Zahabi, E. S. Effects of Alpha-Lipoic Acid Supplementation on Cardiovascular Disease Risk Factors in β-Thalassemia Major Patients: A Clinical Trial Crossover Study. *Journal of Blood Medicine* **2020**, *11*, 131.

(4) Laher, I. Diabetes and alpha lipoic acid. *Frontiers in pharmacology* **2011**, *2*, 69.

(5) Fava, A.; Pirritano, D.; Plastino, M.; Cristiano, D.; Puccio, G.; Colica, C.; Ermio, C.; De Bartolo, M.; Mauro, G.; Bosco, D. The effect of lipoic acid therapy on cognitive functioning in patients with Alzheimer's disease. *Journal of neurodegenerative diseases* **2013**, *2013*, 1.

(6) Cheng, Y.; Luo, F.; Zhang, Q.; Sang, Y.; Chen, X.; Zhang, L.; Liu, Y.; Li, X.; Li, J.; Ding, H. α-Lipoic acid alleviates pentetrazol-induced neurological deficits and behavioral dysfunction in rats with seizures via an Nrf2 pathway. *RSC Adv.* **2018**, *8* (8), 4084−4092.

(7) Stowe, R. C.; Sun, Q.; Elsea, S. H.; Scaglia, F. LIPT1 deficiency presenting as early infantile epileptic encephalopathy, Leigh disease, and secondary pyruvate dehydrogenase complex deficiency. *American Journal of Medical Genetics Part A* **2018**, *176* (5), 1184−1189.

(8) Teichert, J.; Kern, J.; Tritschler, H.; Ulrich, H.; Preiss, R. Investigations on the pharmacokinetics of alpha-lipoic acid in healthy volunteers. *International journal of clinical pharmacology and therapeutics* **1998**, *36* (12), 625−628.

(9) Banik, S.; Halder, S.; Sato, H.; Onoue, S. Self-emulsifying drug delivery system of (R)-α-lipoic acid to improve its stability and oral absorption. *Biopharmaceutics & Drug Disposition* **2021**, *42* (5), 226−233.

(10) Çoban, Ö.; Yıldırım, S.; Bakır, T. Alpha-Lipoic Acid and Cyanocobalamin Co-Loaded Nanoemulsions: Development, Characterization, and Evaluation of Stability. *Journal of Pharmaceutical Innovation* **2021**, in press. DOI: 10.1007/s12247-020-09531-4

(11) Gogoi, P.; Dutta, A.; Ramteke, A.; Maji, T. K. Preparation, characterization and cytotoxic applications of curcumin-(±) α-lipoic acid coloaded phosphorylated chitosan nanoparticles in MDA MB 231 breast cancer cell line. *Polym. Adv. Technol.* **2020**, *31* (11), 2827−2841.

(12) Wang, J.; Tang, J.; Zhou, X.; Xia, Q. Physicochemical characterization, identification and improved photo-stability of alpha-lipoic acid-loaded nanostructured lipid carrier. *Drug development and industrial pharmacy* **2014**, *40* (2), 201−210.

(13) Bao, Y.; Guo, Y.; Zhuang, X.; Li, D.; Cheng, B.; Tan, S.; Zhang, Z. D-α-tocopherol polyethylene glycol succinate-based redox-sensitive paclitaxel prodrug for overcoming multidrug resistance in cancer cells. *Mol. Pharmaceutics* **2014**, *11* (9), 3196−3209.

(14) Cao, N.; Feng, S.-S. Doxorubicin conjugated to d-α-tocopheryl polyethylene glycol 1000 succinate (TPGS): conjugation chemistry, characterization, in vitro and in vivo evaluation. *Biomaterials* **2008**, *29* (28), 3856−3865.

(15) Sheng, S.; Zhang, T.; Li, S.; Wei, J.; Xu, G.; Sun, T.; Chen, Y.; Lu, F.; Li, Y.; Yang, J. Targeting vitamin E TPGS−cantharidin conjugate nanoparticles for colorectal cancer therapy. *RSC Adv.* **2015**, *5* (66), 53846−53856.

(16) Khare, V.; Sakarchi, W. A.; Gupta, P. N.; Curtis, A. D.; Hoskins, C. Synthesis and characterization of TPGS−gemcitabine prodrug micelles for pancreatic cancer therapy. *RSC Adv.* **2016**, *6* (65), 60126−60137.

(17) Tavares Luiz, M.; Delello Di Filippo, L.; Carolina Alves, R.; Sousa Araujo, V. H.; Lobato Duarte, J.; Maldonado Marchetti, J.; Chorilli, M. The use of TPGS in drug delivery systems to overcome biological barriers. *Eur. Polym. J.* **2021**, *142*, 110129.

(18) Kumari, S.; Sharma, P.; Mazumder, A. G.; Rana, A. K.; Sharma, S.; Singh, D. Development and validation of chemical kindling in adult zebrafish: A simple and improved chronic model for screening of antiepileptic agents. *Journal of Neuroscience Methods* **2020**, *346*, 108916.

(19) Najib, N. H.; Nies, Y. H.; Abd Halim, S. A.; Yahaya, M. F.; Das, S.; Lim, W. L.; Teoh, S. L. Modeling Parkinson's Disease in Zebrafish. *CNS & Neurological Disorders-Drug Targets (Formerly Current Drug Targets-CNS & Neurological Disorders)* **2020**, *19* (5), 386−399.

(20) Babin, P. J.; Goizet, C.; Raldúa, D. Zebrafish models of human motor neuron diseases: advantages and limitations. *Progress in neurobiology* **2014**, *118*, 36−58.

(21) Lu, C.; Kim, B. M.; Lee, D.; Lee, M. H.; Kim, J. H.; Pyo, H.-B.; Chai, K. Y. Synthesis of lipoic acid−peptide conjugates and their effect on collagen and melanogenesis. *European journal of medicinal chemistry* **2013**, *69*, 449−454.

(22) Sharma, P.; Kumari, S.; Sharma, J.; Purohit, R.; Singh, D. Hesperidin interacts with CREB-BDNF signaling pathway to suppress pentylenetetrazole-induced convulsions in zebrafish. *Frontiers in pharmacology* **2021**, *11*, 2178.

(23) Mazumder, A. G.; Kumari, S.; Singh, D. Anticonvulsant action of a selective phosphatidylinositol-3-kinase inhibitor LY294002 in pentylenetetrazole-mediated convulsions in zebrafish. *Epilepsy research* **2019**, *157*, 106207.

(24) Sharma, S.; Rana, A. K.; Sharma, A.; Singh, D. Inhibition of Mammalian Target of Rapamycin Attenuates Recurrent Seizures Associated Cardiac Damage in a Zebrafish Kindling Model of Chronic Epilepsy. *Journal of Neuroimmune Pharmacology* **2021**, in press. DOI: 10.1007/s11481-021-10021-8

(25) Rana, A. K.; Sharma, S.; Saini, S. K.; Singh, D. Rutin protects hemorrhagic stroke development via supressing oxidative stress and inflammatory events in a zebrafish model. *Eur. J. Pharmacol.* **2022**, *925*, 174973.

(26) Guo, Y.; Niu, B.; Song, Q.; Zhao, Y.; Bao, Y.; Tan, S.; Si, L.; Zhang, Z. RGD-decorated redox-responsive d-α-tocopherol polyethylene glycol succinate−poly (lactide) nanoparticles for targeted drug delivery. *J. Mater. Chem. B* **2016**, *4* (13), 2338−2350.

(27) Dhaundiyal, A.; Jena, S. K.; Samal, S. K.; Sonvane, B.; Chand, M.; Sangamwar, A. T. Alpha-lipoic acid−stearylamine conjugate-based solid lipid nanoparticles for tamoxifen delivery: formulation, optimization, in-vivo pharmacokinetic and hepatotoxicity study. *J. Pharm. Pharmacol.* **2016**, *68* (12), 1535−1550.

(28) Saneja, A.; Sharma, L.; Dubey, R. D.; Mintoo, M. J.; Singh, A.; Kumar, A.; Sangwan, P. L.; Tasaduq, S. A.; Singh, G.; Mondhe, D. M. Synthesis, characterization and augmented anticancer potential of

https://doi.org/10.1021/acs.jafc.2c01685
J. Agric. Food Chem. XXXX, XXX, XXX−XXX

PEG-betulinic acid conjugate. *Materials Science and Engineering: C* **2017**, *73*, 616−626.
(29) Hsieh, P.-W.; Al-Suwayeh, S. A.; Fang, C.-L.; Lin, C.-F.; Chen, C.-C.; Fang, J.-Y. The co-drug of conjugated hydroquinone and azelaic acid to enhance topical skin targeting and decrease penetration through the skin. *Eur. J. Pharm. Biopharm.* **2012**, *81* (2), 369−378.
(30) Li, D.; Liu, S.; Zhu, J.; Shen, L.; Zhu, H. Folic acid modified TPGS as a novel nano-micelle for delivery of nitidine chloride to improve apoptosis induction in Huh7 human hepatocellular carcinoma. *BMC Pharmacology and Toxicology* **2021**, *22* (1), 1−11.
(31) Ruchika; Sharma, A.; Saneja, A. Zebrafish as a powerful alternative model organism for preclinical investigation of nano-medicines. *Drug Discovery Today* **2022**, *27*, 1513.
(32) Igartúa, D. E.; Azcona, P. L.; Martinez, C. S.; del Valle Alonso, S.; Lassalle, V. L.; Prieto, M. J. Folic acid magnetic nanotheranostics for delivering doxorubicin: toxicological and biocompatibility studies on Zebrafish embryo and larvae. *Toxicology and applied pharmacology* **2018**, *358*, 23−34.
(33) Yi, H.; Zhou, X.; Zhou, C.; Yang, Q.; Jia, N. Liquid exfoliated biocompatible WS 2@ BSA nanosheets with enhanced theranostic capacity. *Biomaterials Science* **2021**, *9* (1), 148−156.
(34) Huang, R.-Q.; Bell-Horner, C. L.; Dibas, M. I.; Covey, D. F.; Drewe, J. A.; Dillon, G. H. Pentylenetetrazole-induced inhibition of recombinant γ-aminobutyric acid type A (GABAA) receptors: mechanism and site of action. *Journal of Pharmacology and Experimental Therapeutics* **2001**, *298* (3), 986−995.
(35) Liu, R.; Wu, S.; Guo, C.; Hu, Z.; Peng, J.; Guo, K.; Zhang, X.; Li, J. Ibuprofen exerts antiepileptic and neuroprotective effects in the rat model of pentylenetetrazol-induced epilepsy via the COX-2/NLRP3/IL-18 pathway. *Neurochem. Res.* **2020**, *45* (10), 2516−2526.
(36) Baraban, S. C.; Taylor, M.; Castro, P.; Baier, H. Pentylenetetrazole induced changes in zebrafish behavior, neural activity and c-fos expression. *Neuroscience* **2005**, *131* (3), 759−768.
(37) Kumari, S.; Mazumder, A. G.; Bhardwaj, A.; Singh, D. Early α-linolenic acid exposure to embryo reduces pentylenetetrazol-induced seizures in zebrafish larva. *Prostaglandins, Leukotrienes and Essential Fatty Acids* **2019**, *143*, 15−20.
(38) Dang, J.; Paudel, Y. N.; Yang, X.; Ren, Q.; Zhang, S.; Ji, X.; Liu, K.; Jin, M. Schaftoside suppresses pentylenetetrazol-induced seizures in zebrafish via suppressing apoptosis, modulating inflammation, and oxidative stress. *ACS chemical neuroscience* **2021**, *12* (13), 2542−2552.
(39) Jin, M.; Zhang, B.; Sun, Y.; Zhang, S.; Li, X.; Sik, A.; Bai, Y.; Zheng, X.; Liu, K. Involvement of peroxisome proliferator-activated receptor γ in anticonvulsant activity of α-asaronol against pentylenetetrazole-induced seizures in zebrafish. *Neuropharmacology* **2020**, *162*, 107760.
(40) Dalle-Donne, I.; Rossi, R.; Giustarini, D.; Milzani, A.; Colombo, R. Protein carbonyl groups as biomarkers of oxidative stress. *Clinica chimica acta* **2003**, *329* (1−2), 23−38.
(41) Zheng, Y.-M.; Chen, B.; Jiang, J.-D.; Zhang, J.-P. Syntaxin 1B mediates berberine's roles in epilepsy-like behavior in a pentylenetetrazole-induced seizure zebrafish model. *Frontiers in Molecular Neuroscience* **2018**, *11*, 378.
(42) Zhang, J.; Zhang, D.; McQuade, J. S.; Behbehani, M.; Tsien, J. Z.; Xu, M. C-fos regulates neuronal excitability and survival. *Nature genetics* **2002**, *30* (4), 416−420.
(43) Alachkar, A.; Azimullah, S.; Lotfy, M.; Adeghate, E.; Ojha, S. K.; Beiram, R.; Łażewska, D.; Kieć-Kononowicz, K.; Sadek, B. Antagonism of histamine H3 receptors alleviates pentylenetetrazole-induced kindling and associated memory deficits by mitigating oxidative stress, central neurotransmitters, and c-fos protein expression in rats. *Molecules* **2020**, *25* (7), 1575.
(44) Siddiqui, M. A.; Akhter, J.; Bashir, D. J.; Manzoor, S.; Rastogi, S.; Arora, I.; Aggarwal, N. B.; Samim, M. Resveratrol loaded nanoparticles attenuate cognitive impairment and inflammatory markers in PTZ-induced kindled mice. *International Immunopharmacology* **2021**, *101*, 108287.

https://doi.org/10.1021/acs.jafc.2c01685
J. Agric. Food Chem. XXXX, XXX, XXX−XXX

International Journal of Biological Macromolecules 264 (2024) 130623

Contents lists available at ScienceDirect

International Journal of Biological Macromolecules

journal homepage: www.elsevier.com/locate/ijbiomac

Orally fast dissolving α-lipoic acid electrospun nanofibers mitigates lipopolysaccharide induced inflammation in RAW 264.7 macrophages

Ruchika, Neha Bhardwaj, Ankit Saneja *

Formulation Laboratory, Dietetics and Nutrition Technology Division, CSIR-Institute of Himalayan Bioresource Technology, Palampur 176061, Himachal Pradesh, India
Academy of Scientific and Innovative Research (AcSIR), Ghaziabad 201002, India

ARTICLE INFO

Keywords:
Lipoic acid
Methyl-beta-cyclodextrin
Pullulan
Inclusion complex
Nanofiber
Anti-inflammatory activity

ABSTRACT

α-Lipoic acid (LA), a dietary supplement known for its strong antioxidant and anti-inflammatory potential, faces challenges due to its poor aqueous solubility and thermal instability. To address these issues, herein methyl-beta-cyclodextrin (M-β-CD) was utilized to create inclusion complex (IC) of LA in 1:1 M stoichiometric ratio of M-β-CD to LA. The LA-M-β-CD-IC was further combined with pullulan (PUL), a non-toxic and water-soluble biopolymer, for the development of electrospun nanofibers (NF) by green and sustainable approach. The resulting PUL/LA/M-β-CD NF formed as a self-standing and flexible material with an average diameter of 569 ± 129 nm and encapsulation efficiency of ~86.90 %. The developed NF demonstrated an accelerated release, quick dissolution, and disintegration when exposed to artificial saliva replicating the conditions of oral cavity. PUL/LA/M-β-CD NF attenuated the production of ROS and NO by downregulating pro-inflammatory enzymes (iNOS and COX-2) in lipopolysaccharide (LPS) stimulated RAW 264.7 cells. Moreover, PUL/LA/M-β-CD NF also significantly down-regulated the expression of pro-inflammatory cytokines including TNF-α, IL-6, and IL-1β along with suppression of NF-κB nuclear translocation in comparison to LA (at 250 μM). In nutshell, PUL/LA/M-β-CD NF demonstrated great potential as a rapid disintegrating delivery system for oral anti-inflammatory treatment due to the enhanced physicochemical characteristics of LA.

1. Introduction

Lipoic acid (LA) is a dietary supplement with a double-sulfhydryl structure that acts as a cofactor for enzymatic complexes involved in cellular energy production [1,2]. LA is known to exhibit antioxidant and anti-inflammatory characteristics, by enhancing the functioning of antioxidant enzymes like glutathione reductase and reinstatement of the equilibrium between reduced and oxidized glutathione [3]. Inflammation and oxidative stress are common features observed in various pathological conditions like diabetic polyneuropathy and Alzheimer's disease. These conditions are characterized by the activation of inflammatory pathways, leading to an overproduction of nitric oxide (NO) and reactive oxygen species (ROS) [4]. A recent clinical study also demonstrated that a four-month treatment with LA in patients with type 2 diabetes mellitus led to significant reduction in inflammatory markers (C-reactive protein [CRP], interleukin-6 [IL-6] and tumor necrosis factor-alpha [TNF- α]) [5]. Unfortunately, these exceptional therapeutic potential of LA is limited by certain technological challenges including low aqueous solubility and susceptibility to heat-induced degradation [2].

In recent years, significant progress has been made in nanotechnology to ameliorate the effectiveness of hydrophobic compounds by leveraging their unique biological properties and adaptable structure. These advancements have resulted in the development of various nanoformulations of LA for different applications, including nanoemulsions [6], lipid nanoparticles [7], polymeric nanoparticles [8], polymer-drug conjugates [2] and self-emulsifying delivery systems (SEDS) [9]. Among these, electrospinning technique has gained considerable attention for producing water-soluble nanofibers having capability of delivering bioactive molecules with poor aqueous solubility and thermal stability. These nanofibers offer several advantages such as rapid disintegration, dissolution, and release of the active ingredient, leading to faster onset of action owing to their large surface area, high porosity, and adequate mechanical properties [10]. Additionally, this innovation has opened up possibilities for developing patient-friendly orally disintegrating delivery systems (ODDSs) that cater to

* Corresponding author at: Dietetics and Nutrition Technology Division, CSIR – Institute of Himalayan Bioresource Technology, Palampur, 176061, Himachal Pradesh, India.
E-mail addresses: ankitsaneja@ihbt.res.in, ankitsaneja.ihbt@gmail.com (A. Saneja).

https://doi.org/10.1016/j.ijbiomac.2024.130623
Received 4 September 2023; Received in revised form 2 March 2024; Accepted 2 March 2024
Available online 4 March 2024

individuals who face challenges in chewing, swallowing, bedridden patients as well as paediatric and geriatrics [10]. Polysaccharides and cyclic oligosaccharides, such as pullulan [11], starch [12], chitosan [13], gelatin [14], soy protein [15], cyclodextrin, and their derivatives [16,17], are among the preferred choices for fabricating nanofibers.

Cyclodextrin (CD) inclusion complexes have emerged as a promising method to improve the solubility and stability of hydrophobic bioactive molecules. These cyclic oligosaccharides, derived from starch, consist of α-1,4-linked glucose units with a hydrophilic outer surface and a hydrophobic core. This unique structure allows CDs to form non-covalent hydrogen bonding interactions with hydrophobic bioactive molecules, thereby enhancing their solubility [11]. Moreover, CD inclusion complexes (IC) also improve thermal stability of compounds, impart controlled release and improved unpleasant taste [18]. The complexation of bioactive molecules such as formononetin [18], genistein [19], myricetin [20], curcumin [21], catechin [22], and dihydroartemisinin [23] with cyclodextrins has demonstrated to enhance their solubility and therapeutic efficacy. Further, Pullulan (PUL) is a water soluble linear polysaccharide of maltotriose units, synthesized by fungus named *Aureobasidium pullulans*. This possesses exceptional properties such as biodegradability, edibility, odorlessness, tastelessness, non-mutagenicity, neutrality and non-hygroscopicity [24]. These attributes make pullulan highly versatile for applications in the food, pharmaceutical, and cosmetic industries [10]. The utilization of pullulan has been demonstrated to enhance the electrospinnability of difficult electrospinning systems by altering conductivity, viscosity and surface tension of the solution [25].

In present study, one-step electrospinning technique was utilized to develop PUL/LA/M-β-CD NF for ameliorating the anti-inflammatory activity of LA. The direct NF formation of LA with PUL leads to negligible loading efficiency due to poor aqueous solubility of LA. Therefore, we have chosen M-β-CD as it demonstrated higher phase solubility in comparison to HP-β-CD and native β-CD for IC formation of LA. Moreover, by forming the inclusion complexation it is also possible to create an aqueous electrospinning solution without toxic organic solvents (green and sustainable approach), typically used for hydrophobic molecules during electrospinning [14]. The electrospinning solution was developed by forming complexation of LA with M-β-CD, followed by the addition of 20 % *w/v* PUL. This approach aimed to overcome the hygroscopic nature of CD, enhanced viscosity and mechanical properties of the nanofiber [25]. The developed PUL/LA/M-β-CD NFs were characterized for their structure, morphology, *in vitro* dissolution, disintegration, and release profile. The anti-inflammatory activities of developed NFs and native LA were also evaluated by analysing NO production and ROS generation in LPS-stimulated RAW 264.7 macrophages. The mechanistic insight of developed NFs was explored using qRT-PCR, Western blot and immunostaining.

2. Material and methods

α-Lipoic acid (LA), β-cyclodextrin (β-CD), Methyl-β-cyclodextrin (M-β-CD) and Hydroxypropyl-β-cyclodextrin (HP-β-CD) were purchased from Sigma-Aldrich. Pullulan (PUL) was purchased from Tokyo Chemical Industry (TCI). 2′-7′-Dichlorodihydrofluorescein diacetate (DCF-DA) dye was procured from MP Biomedicals, LLC, France. Griess reagent system and Verso 1-step RT-qPCR Kit, SYBR Green, ROX were procured from Promega and Thermo Fisher Scientific, respectively. All other solvents and reagents used were of analytical grade.

2.1. Matrix assisted laser desorption ionisation/time-of-flight mass spectrometry (MALDI-TOF)

The MALDI-TOF-TOF mass spectrometer (Bruker ultra TOF, USA) was used to determine the average molecular weight of the cyclodextrins (M-β-CD and HP-β-CD). Prior to analysis, 1 μL of CD solution was applied to a metal plate, followed by 1 μL of saturated solution containing α-Cyano-4-hydroxycinnamic acid (CHCA) matrix. In positive ion reflector mode, spectra were captured in the mass range of 700–3500 Da. Flex Analysis software was used to examine the acquired data [19].

2.2. Phase solubility studies

The solubility of LA was analysed using the Higuchi and Conners method [26]. In this experiment, different concentrations (0–12 mM) of β-CD, M-β-CD and HP-β-CD in water were prepared in 2 mL microcentrifuge tubes. Thereafter, an excess amount of LA was added in each tube and incubated at 25 °C for 24 h in IKA® matrix orbital shaker (Delta F2.0, Germany) [27]. After 24 h, the suspensions were centrifuged at 10,000 rpm for 10 min and filtered to remove undissolved LA. The extent of LA solubility was analysed using isocratic method with binary elution system of methanol: 0.01 % TFA water (70:30) at 335 nm wavelength *via* HPLC (Agilent 1260 Inifinity II). The average of three measurements was used to plot the phase solubility graph and fold increase in solubility. The binding constant (Ks) was calculated using the following equation.

$$Ks = \frac{Slope}{S_0\ (1 - Slope)}$$

where, S_0 is the solubility of LA in water without CD. Slope can be derived from the linear equation of phase solubility curve.

2.3. Development of lipoic acid/cyclodextrin inclusion complex pullulan nanofiber

The IC of LA with M-β-CD was prepared by mixing them in 1:1 M stoichiometric ratio (LA: M-β-CD). Initially, M-β-CD (23 % *w/v*) was dissolved in water followed by the addition of LA [10]. The mixture was incubated overnight at room temperature (RT) with continuous stirring, resulting in a clear solution of the inclusion complex. Further, PUL (20 % *w/v*) was incorporated in the LA-M-β-CD IC solution and stirred at RT to get clear solution. The conductivity and viscosity of the solution was also measured using a conductivity meter (deluxe conductivity meter, Model-602) and viscometer (IKA ROTAVISC lo-vi), respectively. The developed solution was filled in 1 mL syringe with stainless-steel needle (27 G) and was subjected for electrospinning (*E*-SPIN NANOTECH, model: Super ES-1) at high voltage (15 kV) with constant flow rate of 0.7 mL/h [27]. The nanofibers were collected on roller covered with aluminum foil positioned 15 cm away from the needle. The humidity and temperature during the electrospinning process was recorded to be ~ 25 % and ~ 20 °C. The blank NF consisting of pure PUL and CD solutions without LA was also prepared using the same protocol.

2.4. Characterization of nanofibers

2.4.1. Morphological analysis of nanofibers using scanning electron microscopy (SEM)

The morphology of the developed NFs was investigated using Scanning electron microscopy (model S-3400 N, Hitachi, Tokyo, Japan). In order to analyse the samples, they were firmly affixed to 25 mm brass stubs using double-sided carbon adhesive tapes. Since the samples lacked conductivity, a thin layer of Au was applied to all samples through sputter coating under vacuum prior to the measurements. The average diameter (AD, mean ± SD) of NFs was determined using ImageJ software based on at least 100 measurements from different locations of micrographs.

2.4.2. Nuclear magnetic resonance spectroscopy (NMR) analysis

The proton nuclear magnetic resonance (^{1}H NMR) spectroscopy was used to analyse the presence and preservation of LA chemical structure during the electrospinning process in NF. Briefly, LA, PUL, M-β-CD, and PUL/LA/M-β-CD NF were dissolved in DMSO-d_6 and measurements

were recorded using a NMR spectrometer equipped with an auto sampler (NMR, AV-600, Bruker, USA). The chemical shift (δ) values were plotted in parts per million (ppm) relative to the tetramethylsilane (TMS) signal (0 ppm).

2.4.3. Fourier transform infrared spectroscopy (FT-IR) analysis

The Fourier transform infrared (FT-IR) spectra of native LA, PUL, M-β-CD, and PUL/LA/M-β-CD NF were recorded in the range of 4000–550 cm^{-1} (PerkinElmer, ES version 10.5.3 software). The samples were analysed using potassium bromide (KBr) pellets compressed with the samples using a hydraulic press before analysis.

2.4.4. Differential scanning calorimetry (DSC) analysis

The thermal behaviour of LA, PUL, M-β-CD, and PUL/LA/M-β-CD NF were analysed by differential scanning calorimeter (DSC, DSC200, Hitachi). Prior to analysis, the 3–5 mg of samples were sealed in chromated aluminum pan and heated from 25 °C to 250 °C at a scanning rate of 10 °C/min under a dry nitrogen flow (flow rate: 50 mL/min). An empty sealed chromated aluminum pan was used as reference.

2.4.5. Thermal gravimetric analysis (TGA) analysis

The thermal degradation behaviour of LA, PUL, M-β-CD, and PUL/LA/M-β-CD NF was recorded using thermogravimetric analyzer (TGA, Mettler Toledo, model: TGA/DSC-I, Columbus, OH, USA). TGA analyses of the samples were recorded from 30 °C to 700 °C at 20 °C/min rate. The measurements were performed in sealed aluminum pans with a blank pan used as a reference.

2.4.6. Powder X-ray diffraction analysis

The diffraction patterns of LA, PUL, M-β-CD, and the PUL/LA/M-β-CD NF were recorded using powder X-ray diffractometer (Rigaku Corporation, Tokyo, Japan). The diffractograms were recorded by scanning the 2θ diffraction angle in the range of 5–60° with a step width resolution of 0.02° and scanning rate of 10°/min.

2.5. Time dependent release of LA

The release profile of PUL/LA/M-β-CD NF was investigated in phosphate-buffered saline (PBS, 20 mL) solution for 12 min. Initially, the NF sample was weighed (equivalent to 10 mg of LA), dissolved in PBS solution and placed on magnetic stirrer at a 200 rpm speed. The aliquots of 0.7 mL were withdrawn at specific time intervals (0, 60, 120 s, up to 720 s) and rest of the solution was replenished with an equal volume of fresh PBS [27]. The dissolved LA content in the samples was analysed using HPLC after filtration. The release test was conducted in triplicate, and the results are reported as the mean ± SD.

2.6. In vitro dissolution and disintegration

The dissolution test was conducted with LA, PUL/LA/M-β-CD NF (2.5 mg equivalent to LA) and blank NF. The samples were placed in glass vials and 5 mL of distilled water was added to each vial while video recording to observe the dissolution process. The disintegration behaviour of PUL/LA/M-β-CD NF and the blank NF were examined in a simulated physiological environment resembling the moist surface of tongue. In brief, a filter paper of appropriate size was placed in a petri dish and moistened with artificial saliva. The artificial saliva was developed using 1.4 mM KH_2PO_4, 16.8 mM Na_2HPO_4, 137 mM NaCl in10 mL water having 6.8 pH [27]. After removing extra synthetic saliva from the petri dish, a piece of PUL/LA/M-β-CD NF or blank NF was positioned in the middle of the filter paper and disintegration processes was captured.

2.7. Cell culture

RAW 264.7 murine macrophages were obtained from the National Centre for Cell Science (NCCS), Pune, India. The cells were revived and cultivated using DMEM media supplemented with 10 % fetal bovine serum (FBS, Gibco, USA) and 1 % antibiotic–antimycotic solution. The cultures were kept at 37 °C with 5 % CO_2 atmosphere in incubator. Further, for experiments, cells were treated with LA and PUL/LA/M-β-CD NF at different concentrations (100 μM, 250 μM, and 500 μM equivalent to LA) for 24 h followed by lipopolysaccharides (LPS, 1 μg/mL) induction for another 24 h.

2.8. In vitro evaluation of anti-inflammatory potential of nanofibers

2.8.1. Cell viability assay

The inhibitory effect of PUL/LA/M-β-CD NF on the growth of RAW 264.7 cells with or without LPS induction was assessed using MTT assay [28]. Briefly, cells were cultivated in 96-well plates at a density of 1×10^4 cells per well and treated with different concentrations of LA and PUL/LA/M-β-CD NF (100 μM, 250 μM, and 500 μM equivalent to LA) for 24 h followed by LPS induction for 24 h. After LPS induction, MTT solution (stock solution of 5 mg/mL) was added to each well and incubated for an additional 4 h at 37 °C. The formazan crystals were dissolved with DMSO after complete removal of culture media and optical density at 570 nm was measured by microplate reader (Infinite® 200 PRO from Tecan). The morphological changes in macrophages after LPS induction and NF treatment were captured using fluorescent cell imager (ZOE™ Fluorescent Cell Imager, Bio-Rad). Percent cell viability was calculated by using following equation:

$$\%Cell\ Viability = \frac{OD_{test}}{OD_{control}} * 100$$

2.8.2. NO production estimation by griess reagent

RAW 264.7 cells were seeded in a 96-well plate with 100 μL of cell suspension containing 1×10^6 cells per well. The cells were pre-treated with different concentrations of LA and PUL/LA/M-β-CD NF (100 μM, 250 μM, and 500 μM equivalent to LA) and incubated at 37 °C for 24 h. After the pre-treatment, the cells were exposed to LPS (1 μg/mL) for 24 h for the production of nitric oxide (NO). After the incubation, 100 μL of the supernatant from each well was collected and equal volume of the Griess reagent was added for NO estimation. Finally, absorbance was measured at 535 nm using microplate reader (Infinite® 200 PRO, Tecan, USA) [29]. The standard curve was prepared using sodium nitrite to calculate the amount of NO production.

2.8.3. Reactive oxygen species analysis

The effect of PUL/LA/M-β-CD NF on LPS induced ROS generation in RAW 264.7 cells was analysed by using carboxy-2,7-dichlorohydrofluorescein diacetate (DCF-DA) dye. After treatment of LA and PUL/LA/M-β-CD NF for 24 h at different concentrations, followed by LPS induction, the adherent cells were washed with PBS and incubated with 20 μM DCF-DA (constituted in PBS, 100 μL) for 30 min at 37 °C [30]. Thereafter, the cells were re-washed with PBS and images were captured using fluorescent microscope (EVOS FL Auto 2 Cell Imaging System, Invitrogen). The quantification of ROS was performed using microplate spectrophotometer (Synergy-H1, hybrid reader, Bio-Tek® 275) by measuring the fluorescence intensity at 488 nm (excitation) and 535 nm (emission).

2.8.4. qRT-PCR of pro-inflammatory enzyme and cytokine genes

RAW 264.7 cells were plated in a 6-well plate with 1 mL of cell suspension containing 1×10^6 cells per well. The cells were treated with LA and PUL/LA/M-β-CD NF (250 μM equivalent to LA) for 24 h followed by LPS (1 μg/mL) induction for another 24 h at 37 °C. Total RNA isolation was performed using TRIzol reagent (Ambion, Life technologies) and chloroform. The concentration and purity of RNA was assessed by nanodrop quantification using NanoDrop™ One/OneC Microvolume UV–Vis Spectrophotometer (Thermo Fisher Scientific, MA, USA). Verso

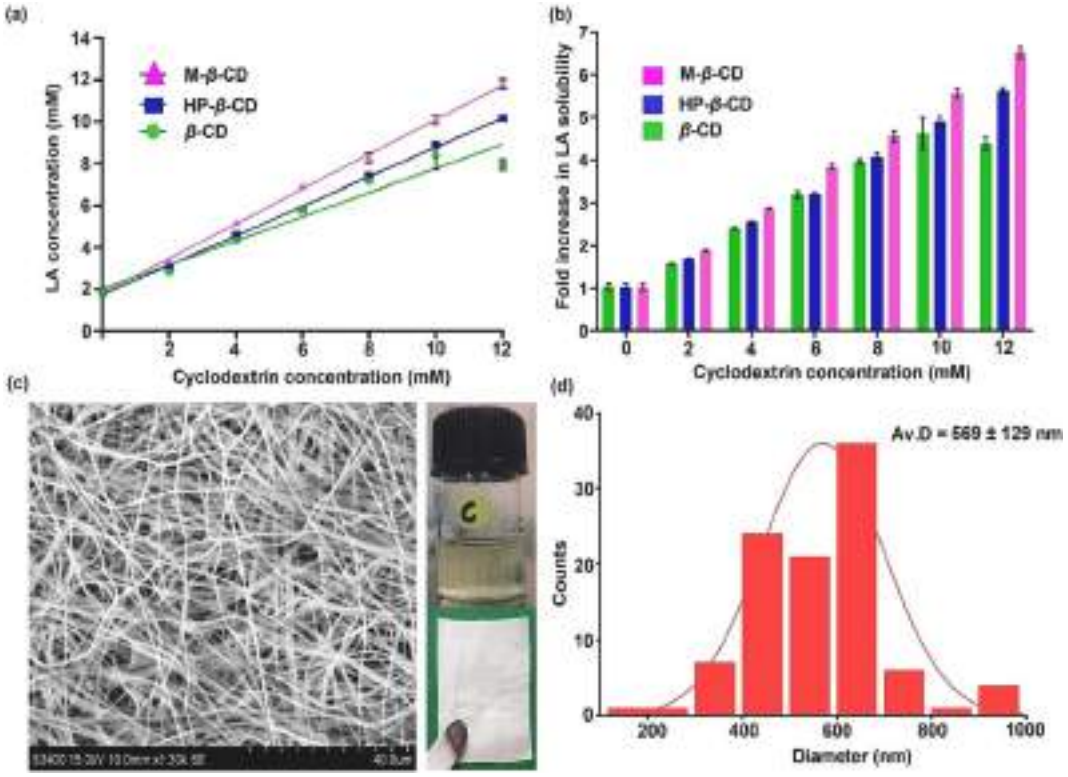

Fig. 1. (a) Phase solubility curve and (b) fold increase in solubility of α-Lipoic acid (LA) with increasing molar concentration (0–12 mM) of β-CD (green colour); Hydroxypropyl- β-cyclodextrin (HP-β-CD; Navy blue colour) and Methyl-β-cyclodextrin (M-β-CD; magenta colour). (c) Scanning electron microscope image and (d) average fibre size distribution of PUL/LA/M-β-CD NF. (For interpretation of the references to colour in this figure legend, the reader is referred to the web version of this article.)

1-step RT-qPCR Kit with SYBR Green and ROX, and CFX Opus Real-Time PCR Systems was used for conducting qRT-PCR of targeted genes. The samples were amplified by 30 cycles of 95 °C denaturation for 15 s, 55 °C annealing for 30 s, and 72 °C elongation for 30 s with initial denaturation step at 95 °C for 5 min. Specific primers for the targeted genes, including COX-2, iNOS, IL-6, IL-1β, TNF-α, and β-actin were used for PCR amplification of cDNA. The relative mRNA expressions were quantified using $2^{-\Delta\Delta Ct}$ method and β-actin was used as housekeeping gene to normalize the mRNA expression. The primer sequences of β-actin, IL-1β, TNF-α, IL-6, iNOS and COX-2 was constructed by Primer express software (Supplementary information Table S1).

2.8.5. Western blot of primary pro-inflammatory enzyme (COX-2)

The pro-inflammatory enzyme, COX-2 protein expression was analysed by western botting. Briefly, RAW 264.7 cells were seeded in a six-well plate with 1 mL of media per well, containing 1×10^6 cells. Cells were treated with LA and PUL/LA/M-β-CD NF solution (equivalent to 250 μM of LA) for 24 h, followed by LPS (1 μg/mL) induction for another 24 h at 37 °C. Following incubation, the cells were collected, washed twice with cold PBS and lysed with RIPA buffer and PIC. The cell lysates were freeze thawed for protein extraction which were further collected and centrifuged at 14,000 rpm for 10 min at 4 °C. The Bradford assay was used to calculate the protein concentrations [31].

The extracted proteins (30 μg/lane) were fractionated by 10 % SDS-PAGE gel, transferred to PVDF membrane using semi-dry trans-blotter system. Bovine serum albumin (BSA, 3 % in TBST) was used to block membranes for 1 h at RT. The blots were incubated with primary antibodies, specifically anti-COX-2 (1:1000) (Cell Signalling Technology Inc., Beverly, MA, USA) and anti-β-actin (Elabscience), overnight at 4 °C. After incubation, membrane was washed with TBST and incubated with a secondary antibody, anti-rabbit IgG HRP conjugated antibody (1:25,000) for another 1 h at RT. After washing with 1× TBST, the protein bands were visualized using an enhanced chemiluminescence (ECL) substrate and image was captured using Azure c300 Gel imager. The bands were quantified using ImageJ software and normalised by the bands of β-actin.

2.8.6. NF-κB protein translocation assay

The effect of PUL/LA/M-β-CD NF on nuclear localization of NF-κB was examined through immunofluorescence staining. Macrophages were exposed with LA and PUL/LA/M-β-CD NF (equivalent to 250 μM of LA) for 12 h followed by LPS induction for 6 h. After washing with PBS, cells were fixed with 4 % paraformaldehyde (40 min. at RT) and permeabilized with 0.25 % Triton X-100 (20 min. at RT). Afterwards, the cells were incubated in blocking solution (5 % BSA) for 1 h and treated with primary antibody (anti-NF-κB p65 antibody, L8F6, Cell Signalling Technology Inc., Beverly, MA, USA) at a dilution of 1:800. A secondary antibody labelled with Alexa Fluor 488 (Cell Signalling Technology Inc., Beverly, MA, USA), particularly directed against anti-mouse IgG, was used to visualize the translocation of NF-κB [29]. The nuclei were stained with DAPI (2 μg/mL) for 10 min. Following another round of PBS washing, images were captured using fluorescence microscope (EVOS FL Auto 2 Cell Imaging System, Invitrogen).

2.9. Statistics analysis

The results were displayed as the mean and standard deviation (SD) for three separate values ($n = 3$). One-way analysis of variance with a Tukey's *post hoc* test was used to determine the significant difference between the means of each group using the graph pad prism software 9 (GraphPad Software Inc., CA, USA) at significance level of $p < 0.05$.

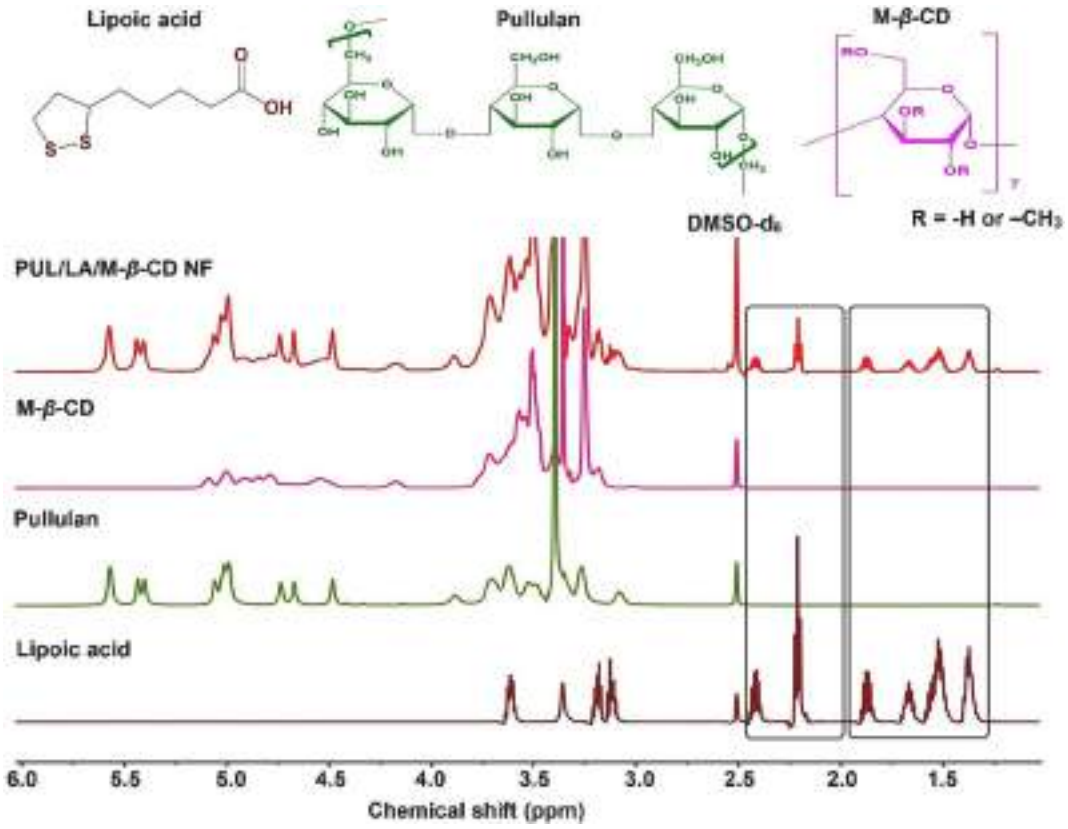

Fig. 2. Proton NMR spectra of Lipoic acid (LA), Pullulan (PUL), Methyl-β-cyclodextrin (M-β-CD) and Pullulan/lipoic acid/M-β-CD nanofiber (PUL/LA/M-β-CD NF) in DMSO-d_6 solvent. Highlighted portion represents the characteristic peaks of LA observed in both LA and PUL/LA/M-β-CD NF, indicating the successful encapsulation and preservation of LA during electrospinning process.

3. Results and discussion

3.1. Mass spectra of M-β-CD and HP-β-CD

The mass spectra of both M-β-CD as well as HP-β-CD was recorded to determine the degree of substitution and average molecular weight before conducting phase solubility of LA with CD derivatives. MALDI spectra of M-β-CD demonstrated peak difference of 15 Da corresponding to the molecular weight of one methyl substitution with average molecular weight of 1302.764 Da (Fig. S1 a). Likewise, MALDI spectra of HP-β-CD demonstrated peak difference of 58 Da corresponding to the molecular weight of one hydroxypropyl substitution and average molecular weight of 1482.789 Da (Fig. S1b). From the MALDI spectra of both CDs (M-β-CD and HP-β-CD) and molecular weight of β-CD (1135 g/mol), this can be inferred that degree of substitution lies in between 8-16 for M-β-CD and 2–9 for HP-β-CD (Supplementary information; Table S2). The observed average molecular weight of both M-β-CD and HP-β-CD were in correlation with the previously conducted mass studies [19,32].

3.2. Phase solubility studies: molar stoichiometric ratio and stability constant

The phase solubility studies of LA with β-CD, M-β-CD and HP-β-CD were conducted to determine the solubility, molar stoichiometric ratio, stability constant and to choose the best CD derivative for the development of IC. The results of phase solubility revealed linear (A_L – type curve) increase in solubility of LA ranked in order M-β-CD ($r^2 = 0.999$) > HP-β-CD ($r^2 = 0.998$) > β-CD ($r^2 = 0.952$), which represents 1:1 M stoichiometric ratio (host: guest molecule) of LA with all CDs as per Higuchi and Connors (Fig. 1 a & b). Further, stability constant (K_s, M^{-1}) of ICs, calculated from slope of linear phase solubility plots, revealed highest value in case of M-β-CD (2523.8 M^{-1}) followed by HP-β-CD (1257.4 M^{-1}) and β-CD (717.4 M^{-1}). The higher value of stability constant usually indicates the higher stability and better ability of inclusion complex formation [33]. Therefore, on the basis of these results, M-β-CD was the preferable choice for IC formation of LA with highest solubility and stability constant.

3.3. Electrospinning of nanofibers and morphological analysis

In this study, PUL/LA/M-β-CD NF was developed by using one-step electrospinning technique, which offers the advantage of incorporating higher concentrations of cyclodextrin (23 % *w/v*) leading to encapsulation/solubilisation of higher amount of bioactive molecules [10]. LA-M-β-CD IC was prepared by overnight incubation and then PUL (20 % w/v) was directly added to the inclusion complex solution resulting in the formation of clear and homogenous system. The viscosity and conductivity plays crucial role in the development and morphology of NFs, therefore, bot parameters of electrospinning solution were recorded. The value of viscosity and conductivity of PUL/LA/M-β-CD NF solution was determined as 1332 ± 12 mPa.s and 1.28 ± 0.008 S/cm, respectively. One-step electrospinning technique imparts the advantage of enhanced encapsulation of IC inside PUL NFs with entrapment efficiency of ~86.90 %. The PUL/LA/M-β-CD NF was successfully developed from electrospinning solutions and demonstrated uniform, bead and defect free morphology with average NF diameter of 569 ± 129 nm (Fig. 1 c & d). This has been observed that low viscosity and high conductivity of the solution usually results in thinner fibres as compared to its counterpart [10,27,34]. The deviation of PUL/LA/M-β-CD NF size from blank NFs (127 ± 23 nm; 1229.3 ± 50.2 mPa.s) may be due to encapsulation of LA-M-β-CD IC as well as increase in viscosity of PUL/LA/M-β-CD NF solution (Supplementary information; Table S3).

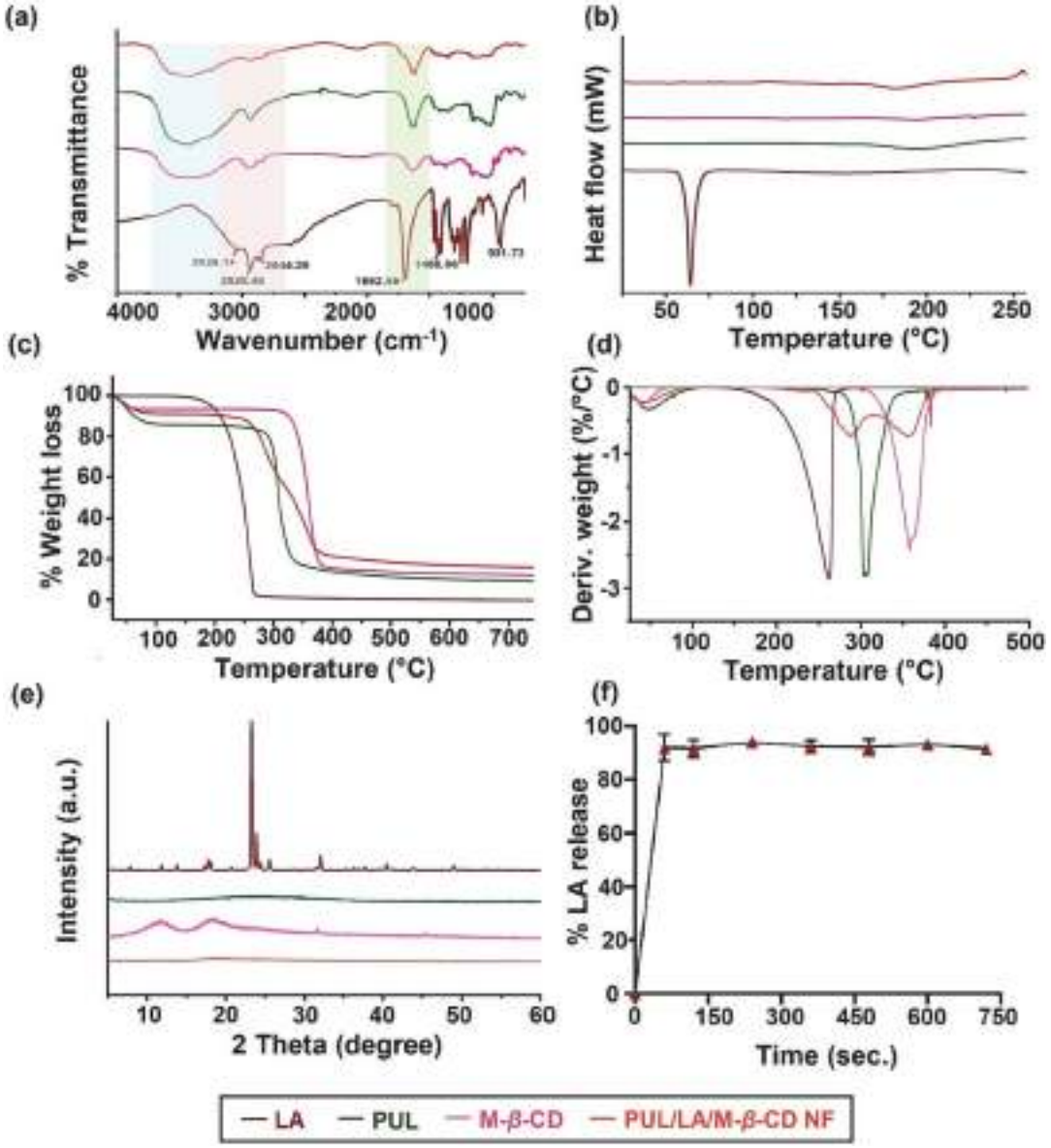

Fig. 3. Structural characterization and release profile of PUL/LA/M-β-CD NF. (a) FT-IR spectra, (b) DSC thermogram, (d) TGA thermogram, (d) derivative weight (%) loss curve and (e) XRD diffractogram of LA (brown), PUL (green), M-β-CD (magenta) and PUL/LA/M-β-CD NF (red). Highlighted portions in FT-IR spectra represent the masking, shifting and broadening of LA bands after inclusion complex and nanofiber formation. (f) *In vitro* time dependent release profile of LA from PUL/LA/M-β-CD NF expressed in cumulative % release over the period of 12 min. (For interpretation of the references to colour in this figure legend, the reader is referred to the web version of this article.)

3.4. Structural characterization of PUL/LA/M-β-CD nanofiber

3.4.1. Nuclear magnetic resonance spectroscopy analysis

The presence and successful encapsulation of LA within PUL/LA/M-β-CD NFs were analysed by ^{1}H NMR spectra of LA, PUL, M-β-CD, and PUL/LA/M-β-CD NF individually. The distinctive peaks corresponding to the LA observed in the ^{1}H NMR spectra of the NF provided the evidence of LA being loaded into the PUL/LA/M-β-CD NF (Fig. 2) [2]. Notably, the characteristic peaks of LA in the spectra of both LA and PUL/LA/M-β-CD NF were identical, indicating the preservation of LA's chemical structure throughout the entire electrospinning process, thus ensuring its protection and stability [10,27].

3.4.2. Fourier transform infrared spectroscopy analysis

The FT-IR spectra of LA, PUL, M-β-CD and PUL/LA/M-β-CD NF were performed to investigate the formation of ICs and possible molecular interactions between the guest (LA) and host molecules (M-β-CD) (Fig. 3 a) [35]. The FT-IR spectrum of LA displayed absorption bands at 1692.66 cm^{-1} and 2928.46 cm^{-1}, which corresponded to the stretching vibrations of the C═O bond and the O—H bond, respectively [2,27]. The spectrum of M-β-CD exhibited a characteristic band in the range of 3400–3700 cm^{-1}, indicating the presence of free -OH groups [36]. While PUL demonstrated a similar pattern to M-β-CD due to the presence of $\alpha(1 \rightarrow 4)$ linked glucopyranose units. Notable peaks in the PUL spectrum included O—H stretching (3414.12 cm^{-1}), C—H stretching (2929 cm^{-1}), H–O–H bending (1638.12 cm^{-1}), and C—O stretching (1200–1000 cm^{-1}) [11]. The peaks at 931 cm^{-1}, 861 cm^{-1}, and 756 cm^{-1} corresponds to the α-(1,6) glycosidic bonds, α-glucopyranosyl units, and α-(1,4) linkages, respectively [24]. The FT-IR spectrum of PUL/LA/M-β-CD NF demonstrated shifting (*e.g.*, from 1708 cm^{-1} to 1809 cm^{-1}) and masking of characteristic LA peaks because of M-β-CD and PUL peaks at similar regions [27]. However, no additional peaks

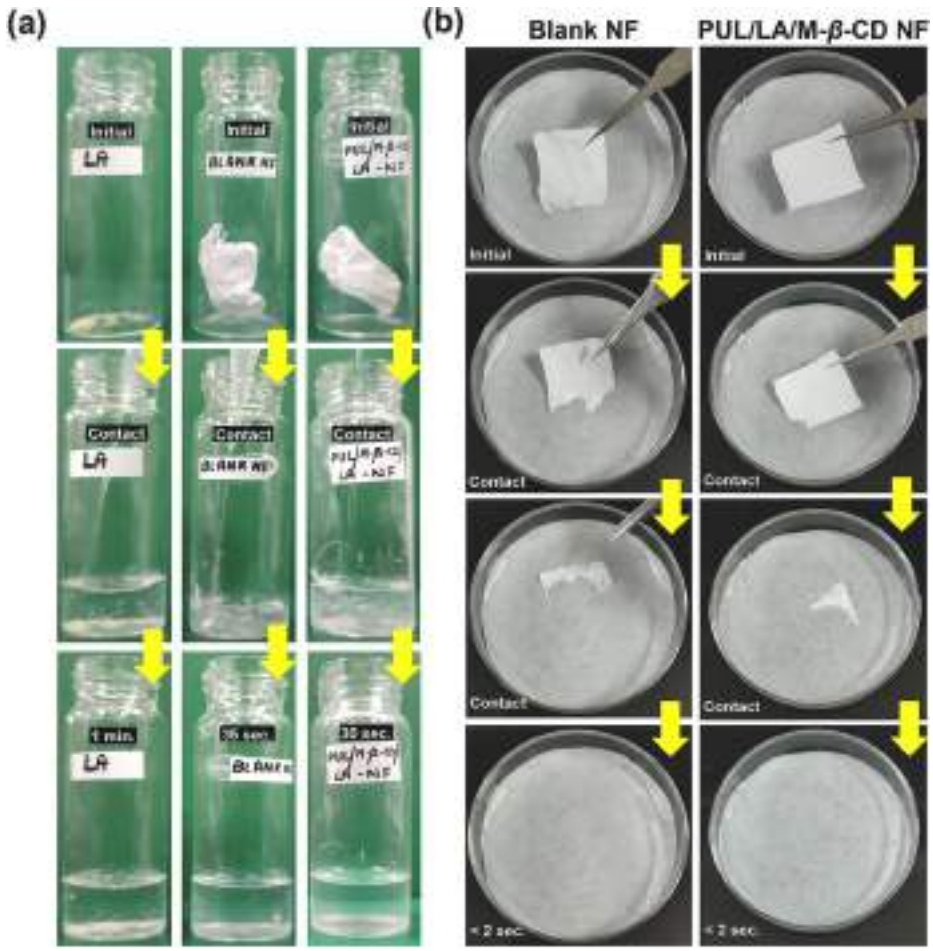

Fig. 4. Dissolution and disintegration behaviour of PUL/LA/M-β-CD NF. (a) Dissolution behaviour of PUL/LA/M-β-CD NF in comparison to blank NF and native LA in 5 mL distilled water. (b) Disintegration behaviour of PUL/LA/M-β-CD NF in comparison to blank NF in artificial saliva.

were observed in the NF spectra, indicating absence of new chemical interactions.

3.4.3. *Differential scanning calorimetry analysis*

DSC analysis was used to further characterize the IC formation and encapsulation of LA inside NF. The DSC thermogram of LA exhibited a sharp endothermic peak at ~64 °C, representing its melting point and crystalline nature [27,33] (Fig. 3 b). Conversely, PUL and NFs displayed broad endothermic peaks in the range of 150–250 °C and 150–200 °C, respectively, indicative of dehydration. However, no such peaks were observed in the DSC thermograms of M-β-CD. In DSC thermograms of PUL/LA/M-β-CD NF, the melting peak of LA was not detected, suggesting complete inclusion complexation and encapsulation of LA within the NF.

3.4.4. *Thermal gravimetric analysis*

The TGA thermograms depicted the thermal behaviour of LA, PUL, M-β-CD, and PUL/LA/M-β-CD NF (Fig. 3c). The LA thermogram revealed a single-step degradation process, with 97 % degradation of LA between 160 and 260 °C. In contrast, PUL, M-β-CD, and PUL/LA/M-β-CD NF exhibited a step-wise degradation pattern, starting with minor weight loss (%) below 100 °C, attributed to water evaporation. The main thermal degradation of M-β-CD (~ 85 %) occurred between 300 and 388 °C, while PUL experienced its main degradation (~ 82 %) between 270 and 340 °C. The TGA thermogram of PUL/LA/M-β-CD NF displayed weight losses in multiple steps. The primary weight loss, corresponding to the main degradation of the NF was observed between 250 and 300 °C (39 % degradation) and 300–383 °C (up to 77 % degradation). The derivative weight (%) loss curve of PUL/LA/M-β-CD NF also demonstrated a multi-step weight loss profile, with initial water evaporation below 100 °C, and significant weight (%) loss peaking at approximately 288 °C and 358 °C, attributed to the degradation of LA, followed by PUL and M-β-CD (Fig. 3d). It was worth noting that the NF substantially enhanced the thermal stability of LA by increasing its complete degradation temperature from ~260 °C to 357 °C.

3.4.5. *Powder X-ray diffraction analysis*

The inclusion complexation between LA and M-β-CD NF was further confirmed by P-XRD. The P-XRD spectra of LA, a crystalline molecule, demonstrated distinct peaks at 23.8°, 24.46°, and 25.5° (Fig. 3e) [27]. Both M-β-CD and PUL are amorphous in nature, so their XRD patterns exhibited broad halos without significant diffraction peaks [36,37]. Similarly, the XRD pattern of PUL/LA/M-β-CD NF demonstrated negligible specific diffraction peaks corresponding to crystalline LA. This indicates that the LA molecules were in an inclusion complexed state with M-β-CD and successfully encapsulated in the NF.

3.5. *In vitro time dependent release, disintegration and dissolution behaviour of NF*

The release of LA from PUL/LA/M-β-CD NF was studied over time, and the results were presented as cumulative percentage release (Fig. 3f). The release study demonstrated that PUL/LA/M-β-CD NF dissolves instantly upon contact with water, leading to ~94 % LA release from the NF matrix within 720 s with initial burst release of ~86 % within 60 s. The fast release profile of LA can be attributed to the unique

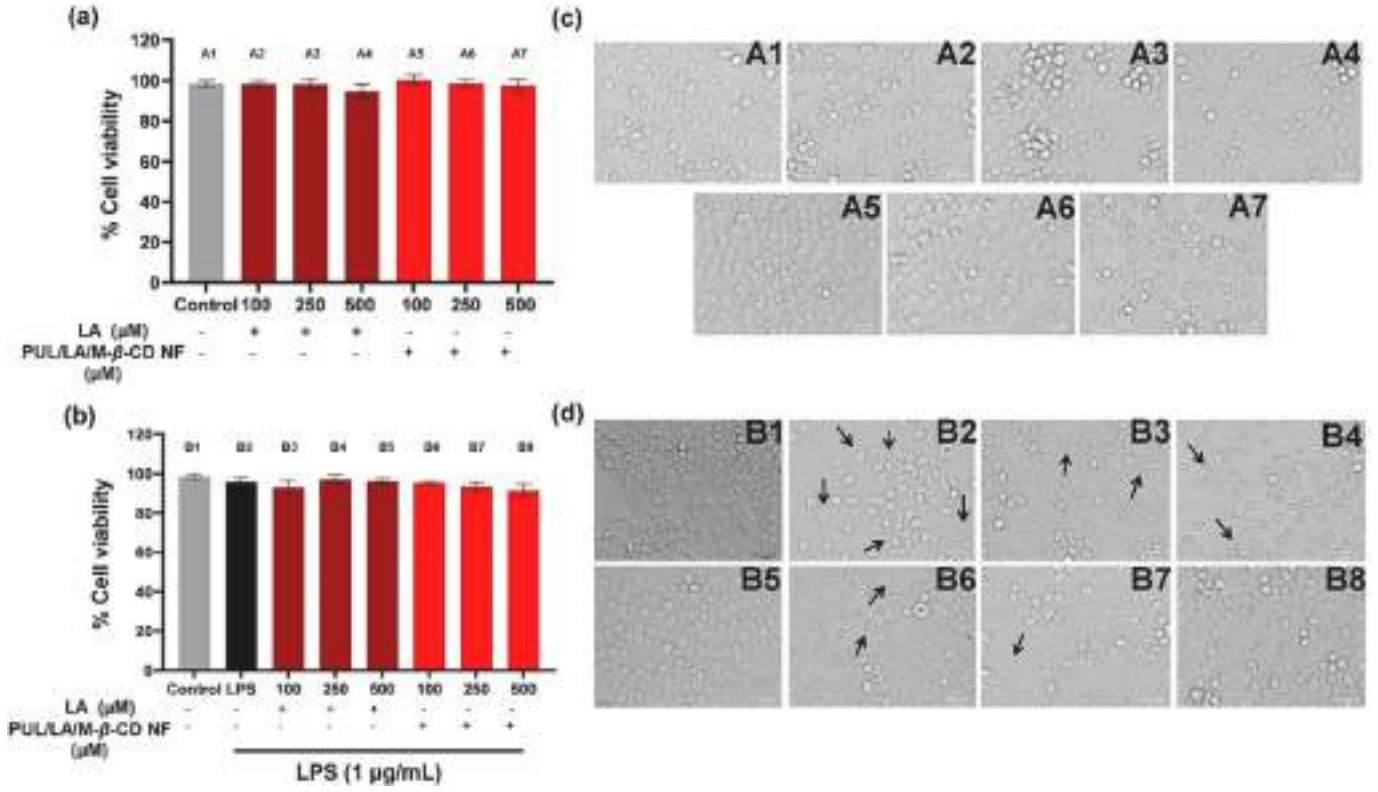

Fig. 5. Effect of PUL/LA/M-β-CD NF on cell viability of RAW 264.7 cells in presence and absence of LPS induction. (a) & (b) cell viability graph of RAW 264.7 cells after 24 h treatment with LA and PUL/LA/M-β-CD NF at different concentration (100, 250 and 500 μM) without and with LPS, respectively. (c) & (d) microscopic images of RAW 264.7 cells representing morphological characteristics without (c) and with LPS induction (d). PUL/LA/M-β-CD NF demonstrated concentration-dependent retention of normal RAW 264.7 cells morphology even after LPS induction (B6, 7 &8). Black headed arrows indicate the morphological changes of macrophages after LPS induction. Images were captured using fluorescent microscope (ZOE™ Fluorescent Cell Imager, Bio-Rad). White line represents 25 μm scale bar.

characteristics of the inclusion complex formation, high surface area, uniform NF size, and porosity [27].

Further, the dissolution behaviour of PUL/LA/M-β-CD NF (equivalent to 2.5 mg LA) was compared with native LA and blank NF. The dissolution study demonstrated that PUL/LA/M-β-CD NF dissolved instantly (within 30 s) due to high water solubility of CD and PUL. In contrast, LA remained undissolved even after 1 min, indicating its poor dissolution profile attributed to its crystalline nature [27] (Fig. 4a).

The disintegration characteristics of both blank and PUL/LA/M-β-CD NF were assessed in a simulated oral environment using filter paper saturated with artificial saliva. Both the blank and PUL/LA/M-β-CD NF exhibited rapid disintegration within 2 s upon contact with artificial saliva (Fig. 4b). The NF's high surface area and porosity facilitate the easy penetration of liquids, contributing to fast disintegration and dissolution of the NF [11]. To summarize, the nano size fibrous structure of PUL/LA/M-β-CD NF ensures the effortless entry of saliva into the developed NF. Furthermore, the formation of ICs between LA and M-β-CD promotes the instantaneous release of LA through rapid dissolution.

3.6. *In vitro evaluation of anti-inflammatory activity of PUL/LA/M-β-CD nanofibers*

3.6.1. *Effect of PUL/LA/M-β-CD NF on viability of RAW 264.7 macrophages*

The cytocompatibility of developed PUL/LA/M-β-CD NF on RAW 264.7 cells was evaluated using MTT cell viability assay. The cell viability results demonstrated that PUL/LA/M-β-CD NF and LA has negligible effect on the viability of RAW 264.7 cells. Moreover, the induction of LPS (1 μg/mL) also demonstrated lesser to no influence on cell viability (Fig. 5a and b). The effect of blank NFs on RAW 264.7 cells were also assessed and exhibited negligible effect on cell viability up to 500 μg/mL (Supplementary information; Fig. S2). The morphological changes in the RAW 264.7 cells were also examined in the control, LPS, LA and PUL/LA/M-β-CD NF-treated groups. The RAW 264.7 cells under normal conditions appeared small, round with smooth surfaces and have homogeneous sizes [38]. The exposure of LA and PUL/LA/M-β-CD NF at different concentrations (100 μM, 250 μM and 500 μM) imposed no significant effect on cell morphology (Fig. 5c). However, exposure to LPS (24 h) resulted in notable morphological changes in the macrophages, such as irregular polygonal shape, increased cell volume and quantity of intracellular granular vesicles, high vacuolation and formation of thin and long dendritic pseudopodia on the cell surface (Fig. 5d [B2]). These modifications demonstrated that LPS significantly induced inflammation in the RAW 264.7 cells [18]. Interestingly, the administration of PUL/LA/M-β-CD NF exhibited protection and prevention of LPS-induced morphological changes in a concentration-dependent manner [Fig. 5d (B6, B7 and B8)]. The PUL/LA/M-β-CD NF at 500 μM demonstrated notable protective effect on the morphology of RAW 264.7 cells in comparison to LPS as well as LA.

3.6.2. *Effect of PUL/LA/M-β-CD NF on LPS induced NO production in RAW 264.7 macrophages*

NO, a pro-inflammatory mediator, is considered as a key marker of inflammation and is triggered by iNOS in macrophages [39]. Its production is a part of the innate immune response in mammals and can indicate the progression of inflammation following exposure to LPS. However, excessive production of NO by triggered macrophages is associated with the development of inflammation-related disorders [40–44]. Therefore, ameliorated effect of PUL/LA/M-β-CD NF on NO

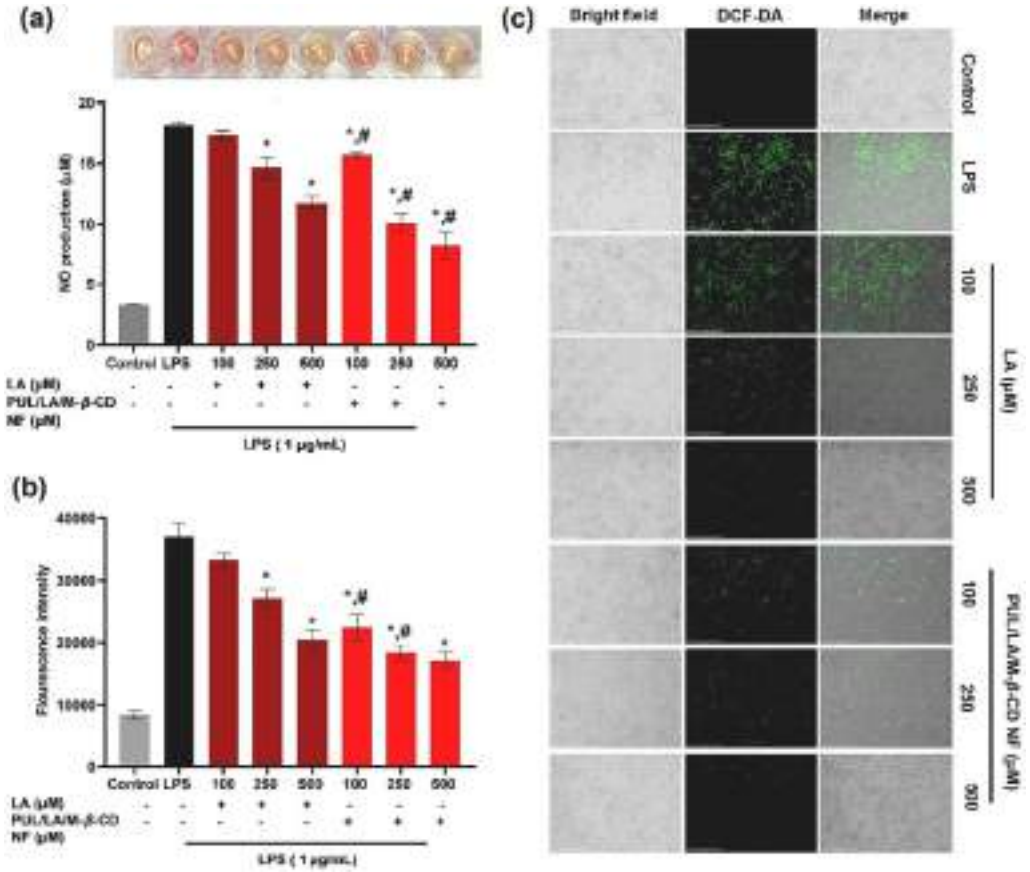

Fig. 6. Effect of PUL/LA/M-β-CD NF on LPS induced NO and ROS production in RAW 264.7 cells after its 24 h treatment followed by 24 h LPS induction. (a) Graph of NO production in RAW 264.7 cells after 24 h treatment with LA and PUL/LA/M-β-CD NF at different concentrations (100, 250 and 500 µM) followed by LPS induction. PUL/LA/M-β-CD NF demonstrated concentration dependent ameliorated effect on LPS induced NO production. The amount of NO production was measured by Griess reagent. (b) Graph of ROS generation in RAW 264.7 cells after 24 h treatment with LA and PUL/LA/M-β-CD NF at different concentrations (100, 250 and 500 µM concentration) followed by LPS induction. Generation of ROS was evaluated by using DCF-DA fluorescent dye and change in fluorescence intensity was plotted as graph. (c) Microscopic images of ROS generation, visualized using DCF-DA green fluorescent dye. Images were captured using fluorescent microscope (EVOS FL Auto 2 Cell Imaging System, Invitrogen). * $p < 0.05$ indicates significant difference in the mean value from LPS group. # $p < 0.05$ indicates significant difference in the mean value of PUL/LA/M-β-CD NF from LA group (with respective concentrations). White line represents 275 µm scale bar. (For interpretation of the references to colour in this figure legend, the reader is referred to the web version of this article.)

production in RAW 264.7 cells was evaluated using Griess reagent. The results demonstrated significantly higher NO production in LPS group as compared to control group. However, PUL/LA/M-β-CD NF treatment demonstrated a significant concentration-dependent reduction in NO production compared to both LPS group as well as LA groups (Fig. 6a).

3.6.3. Effect of PUL/LA/M-β-CD NF on LPS induced ROS generation in RAW 264.7 macrophages

Oxidative stress and inflammatory response are commonly present in various diseases, and both contribute to and accelerate the progression of the illness. ROS promotes inflammation in two ways, either by acting as a redox signal that regulates the duration of inflammation or by accumulating in damaged tissue which further exacerbates the production of inflammatory vesicles [55]. Moreover, ROS can also trigger the NF-κB pathways, leading to the release of pro-inflammatory cytokines [45–47]. Therefore, the study aimed to evaluate the improved effect of PUL/LA/M-β-CD NF on ROS generation in induced RAW 264.7 cells using DCF-DA dye. The results demonstrated significant increase in ROS generation in RAW 264.7 cells upon induction of LPS as compared to the control group. However, PUL/LA/M-β-CD NF demonstrated a concentration-dependent decrease in ROS generation, which was more pronounced in comparison to both LPS and LA groups (Fig. 6b). Microscopic images of ROS visualized using DCF-DA fluorescent dye also demonstrated the efficacy of PUL/LA/M-β-CD NF in significantly decreasing the ROS generation as compared to native LA (Fig. 6c).

3.6.4. Suppressive effect of PUL/LA/M-β-CD NF on mRNA level of pro-inflammatory enzymes/cytokines

The macrophages serve as the initial defence system against infections and play a vital role in protecting the body from various infections [39]. However, excessive activation of macrophages can contribute to the development of inflammatory disorders by generating abundant quantity of pro-inflammatory enzyme and cytokines. This abnormal activation is often triggered by exposure to LPS, a component found in the outer membrane of gram -ve bacteria [48]. LPS is commonly used to study the inflammatory responses in RAW 264.7 cells. These macrophages, when exposed to LPS, have been extensively observed to increase the production pro-inflammatory enzymes like iNOS and COX-2 [38,49]. Both iNOS and COX-2 are crucial enzymes responsible for generating two major inflammatory mediators: NO and PGE2, respectively. In addition, activated macrophages release significant levels of pro-inflammatory cytokines such as TNF-α, IL-1β, and IL-6. These can influence a complex signalling network involved in inflammation. For instance, TNF-α and IL-1β promote neutrophil accumulation and the release of other cytokines, initiating and perpetuating the inflammatory response. On the other hand, IL-6 helps in maintaining tissue balance and regulates the extent of the inflammatory responses [38].

LA possesses promising anti-inflammatory activities by suppressing

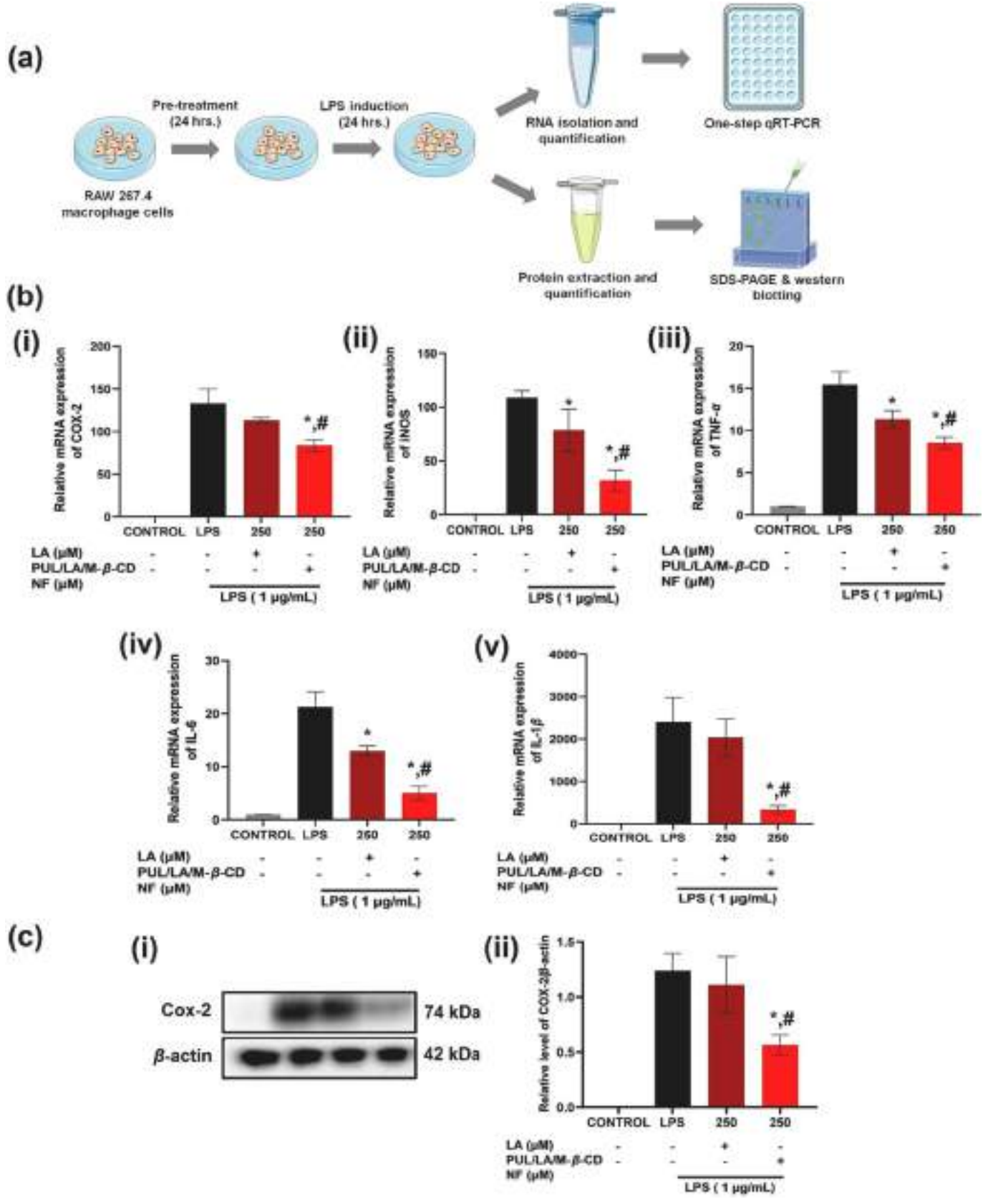

(caption on next page)

Fig. 7. (a) Schematic representation of methodology followed for the treatment, protein and RNA isolation from LPS induced RAW 264.7 cells.
(b) & (c) Suppressive effect of PUL/LA/M-β-CD NF on mRNA level of pro-inflammatory enzymes/cytokines and protein levels of COX-2 in LPS induced RAW 264.7 cells.
mRNA levels of iNOS, COX-2, TNF-α, IL-6 and IL-1β was analysed by qRT-PCR in cells treated with LA and PUL/LA/M-β-CD NF (250 μM equivalent to LA) for 24 h followed by induction of LPS (1 μg/mL) for another 24 h.
Protein expression of COX-2 was analysed by Western blotting in cells treated with LA and PUL/LA/M-β-CD NF (250 μM equivalent to LA) for 24 h followed by induction of LPS (1 μg/mL) for another 24 h.
*$p < 0.05$ indicates significant difference in the mean value from LPS group. #$p < 0.05$ indicates significant difference in the mean value of PUL/LA/M-β-CD NF from LA group (with respective concentrations).

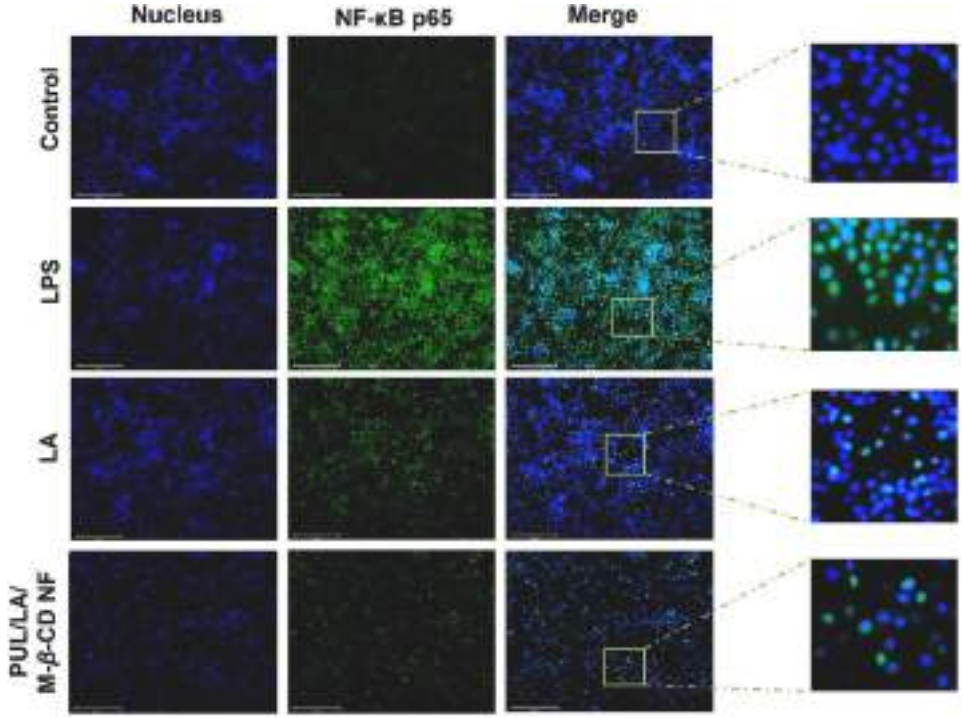

Fig. 8. Inhibitory effect of PUL/LA/M-β-CD NF on LPS-stimulated nuclear translocation of NF-κB in RAW 264.7 cells analysed by fluorescent microscopy. Macrophages were immunostained by Alexa Fluor 488 for NF-κB and DAPI for nuclei staining. Images were captured using fluorescent microscope (EVOS FL Auto 2 Cell Imaging System, Invitrogen). White line represents 125 μm scale bar.

the overexcited expressions of pro-inflammatory enzymes and cytokines [50]. Therefore, the ameliorated effect of PUL/LA/M-β-CD NF on downregulating the mRNA levels of pro-inflammatory enzymes (iNOS and COX-2) and cytokines (TNF-α, IL-1β, and IL-6) was determined by qRT-PCR. The results of qRT-PCR demonstrated that PUL/LA/M-β-CD NF significantly downregulates the mRNA levels of iNOS, COX-2, TNF-α, IL-1β, and IL-6 compared to both LPS and LA (250 μM) group (Fig. 7b).

3.6.5. Suppressive effect of PUL/LA/M-β-CD NF on protein expression of COX-2 in RAW 264.7 macrophages

The ameliorated effect of PUL/LA/M-β-CD NF on protein expression of COX-2 was also evaluated using Western blotting. The results of COX-2 Western blotting demonstrated that PUL/LA/M-β-CD NF treatment significantly suppressed the protein expression of COX-2 in RAW 264.7 cells as compared to the LPS and LA group (250 μM concentration) (Fig. 7c). Moreover, RAW 264.7 cells of control group presented negligible expression of COX-2 protein which is usually observed in LPS untreated cells whereas, a significant upregulation of COX-2 protein expression was observed in LPS group [51,52].

3.6.6. Inhibitory effect of PUL/LA/M-β-CD NF on LPS-stimulated nuclear translocation of NF-κB in RAW 264.7 macrophages

The iNOS and COX-2 matrix proteinases are crucial pro-inflammatory enzymes, and their gene expression is regulated by downstream signalling of NF-κB. NF-κB acts as a transcription factor and plays a vital role in managing the transcription of various inflammation-related genes. Downregulation of NF-κB leads to decrement in generation of pro-inflammatory cytokines such as TNF-α, IL-6, and IL-1β [29,39].

Based on these facts, we further assessed the ability of NF to suppress the nuclear translocation of NF-κB. The results demonstrated that PUL/LA/M-β-CD NF (at 250 μM equivalent to LA) significantly suppresses the nuclear translocation of NF-κB in comparison to LA (Fig. 8).

Multiple prior studies have provided evidence of the anti-inflammatory potential of LA by mitigating the production of NO, ROS and its involvement in abnormal inflammatory processes [5,28]. However, its poor aqueous solubility and thermal instability limits its biological properties and application in food supplement without protection [2]. Nanofiber encapsulating LA-M-β-CD-IC enhanced LA solubility, release, dissolution profile and thermal stability (as evident from phase solubility and DSC/TGA analysis) which may lead to increased cellular uptake of LA and ameliorated anti-inflammatory potential. Overall, PUL/LA/M-β-CD NF exhibited an improved anti-inflammatory activity compared to LA by suppressing LPS-induced NO production, ROS generation, downregulation of pro-inflammatory enzymes, cytokines and inhibition of NF-κB nuclear translocation in RAW 264.7 cells.

4. Conclusion

In summary, the results of this study demonstrated that PUL/LA/M-β-CD NF has significant potential to reduce the levels of NO and ROS in LPS induced RAW 264.7 cells. Additionally, the PUL/LA/M-β-CD NF effectively suppresses the expression of pro-inflammatory enzymes, iNOS and COX 2, which were responsible for NO production, as well as pro-inflammatory cytokines like TNF-α, IL-1β, and IL-6. These beneficial effects were achieved by inhibiting the nuclear transloaction of NF-κB [39]. The anti-inflammatory effect of PUL/LA/M-β-CD NF was more prominent due to the nanoscale properties of the nanofiber, including its large surface area which imparted fast disintegration, dissolution, and release profile to LA. Furthermore, the inclusion complex of M-β-CD significantly enhances the solubility of LA (~ 6.5 times) and encapsulation in PUL NF imparts higher thermal stability. Overall, based on these findings, it can be inferred that PUL/LA/M-β-CD NF has the potential to be a viable choice for augmenting the anti-inflammatory effects of LA.

CRediT authorship contribution statement

Ruchika: Writing – original draft, Methodology, Investigation, Formal analysis. **Neha Bhardwaj:** Writing – original draft, Methodology, Investigation, Formal analysis. **Ankit Saneja:** Writing – review & editing, Supervision, Resources, Project administration, Funding acquisition, Conceptualization.

Declaration of competing interest

The authors declare that they have no known competing financial interests or personal relationships that could have appeared to influence the work reported in this paper.

Data availability

Data will be made available on request.

Acknowledgement

The authors are grateful to Director of CSIR-Institute of Himalayan Bioresource Technology for his unwavering support and encouragement. The authors would like to express their gratitude to the Indian Council of Medical Research (ICMR), New Delhi for providing financial assistance (5/9/1423/2022-Nut). The authors are also grateful to Council of Scientific and Industrial Research, India (CSIR), New Delhi, for their support in the MLP-204 project. R. acknowledges the Council of Scientific and Industrial Research (CSIR), New Delhi, for the fellowship provided (File 31/054(0163)/2020-EMR-I). N. B. acknowledges the Indian Council of Medical Research (ICMR), New Delhi, for the fellowship provided (File no. 3/1/2/220/2021-Nut.). The Authors also extend their acknowledgment to the central instrumentation facility at CSIR-Indian Institute of Integrative Medicine (IIIM) Jammu and CSIR- Institute of Microbial Technology for conducting the FT-IR, and TGA analysis respectively. Fig. 7(a) drawn from the material provided by Servier Medical Art under the Creative Common Attribution 3.0 Unported License. The manuscript bears institutional communication number 5464.

Appendix A. Supplementary data

Supplementary data to this article can be found online at https://doi.org/10.1016/j.ijbiomac.2024.130623.

References

[1] S.-y. Lv, S. He, X.-l. Ling, Y.-q. Wang, C. Huang, J.-r. Long, J.-q. Wang, Y. Qin, H. Wei, C.-Y. Yu, Review of lipoic acid: from a clinical therapeutic agent to various emerging biomaterials, Int. J. Pharm. (2022) 122201. https://doi.org/10.1016/j.ijpharm.2022.122201.

[2] S. Ruchika, P. Kumari, D. Dhiman, A. Singh, Saneja, R-α-lipoic acid conjugated to d-α-tocopherol polyethylene glycol 1000 succinate: synthesis, characterization, and effect on antiseizure activity, J. Agric. Food Chem. 70 (25) (2022) 7674–7682, https://doi.org/10.1021/acs.jafc.2c01685.

[3] D. Tibullo, G. Li Volti, C. Giallongo, S. Grasso, D. Tomassoni, C.D. Anfuso, G. Lupo, F. Amenta, R. Avola, V. Bramanti, Biochemical and clinical relevance of alpha lipoic acid: antioxidant and anti-inflammatory activity, molecular pathways and therapeutic potential, Inflamm. Res. 66 (2017) 947–959, https://doi.org/10.1007/s00011-017-1079-6.

[4] D. Kaur, T. Behl, A. Sehgal, S. Singh, N. Sharma, S. Chigurupati, A. Alhowail, A. Abdeen, S.F. Ibrahim, C. Vargas-De-La-Cruz, Decrypting the potential role of α-lipoic acid in Alzheimer's disease, Life Sci. 284 (2021) 119899, https://doi.org/10.1016/j.lfs.2021.119899.

[5] N.V. Altunina, V.G. Lizogub, O.M. Bondarchuk, Alpha-lipoic acid as a means of influence on systemic inflammation in type 2 diabetes mellitus patients with prior myocardial infarction, J. Med. Life 13(1) (2020) 32. 10.25122/jml-2020-0018.

[6] Ö. Çoban, S. Yıldırım, T. Bakır, Alpha-lipoic acid and cyanocobalamin co-loaded nanoemulsions: development, characterization, and evaluation of stability, J. Pharm. Innov. (2021) 1–11, https://doi.org/10.1007/s12247-020-09531-4.

[7] A. Najafi, H.D. Kia, H. Hamishehkar, Does alpha-lipoic acid–loaded nanostructured lipid carriers improve post-thawed sperm quality and ameliorate apoptosis-related genes of rooster sperm? Poult. Sci. 100 (1) (2021) 357–365, https://doi.org/10.1016/j.psj.2020.10.007.

[8] P. Gogoi, A. Dutta, A. Ramteke, T.K. Maji, Preparation, characterization and cytotoxic applications of curcumin-(±) α-lipoic acid coloaded phosphorylated chitosan nanoparticles in MDA MB 231 breast cancer cell line, Polym. Adv. Technol. 31 (11) (2020) 2827–2841, https://doi.org/10.1002/pat.5009.

[9] S. Banik, S. Halder, H. Sato, S. Onoue, Self-emulsifying drug delivery system of (R)-α-lipoic acid to improve its stability and oral absorption, Biopharm. Drug Dispos. 42 (5) (2021) 226–233, https://doi.org/10.1002/bdd.2277.

[10] A. Celebioglu, N. Wang, M.E. Kilic, E. Durgun, T. Uyar, Orally fast disintegrating cyclodextrin/prednisolone inclusion-complex nanofibrous webs for potential steroid medications, Mol. Pharm. 18 (12) (2021) 4486–4500, https://doi.org/10.1021/acs.molpharmaceut.1c00677.

[11] K. Ertan, A. Celebioglu, R. Chowdhury, G. Sumnu, S. Sahin, C. Altier, T. Uyar, Carvacrol/cyclodextrin inclusion complex loaded gelatin/pullulan nanofibers for active food packaging applications, Food Hydrocoll. 142 (2023) 108864, https://doi.org/10.1016/j.foodhyd.2023.108864.

[12] L.M. Fonseca, C.E. dos Santos Cruxen, G.P. Bruni, Â.M. Fiorentini, E. da Rosa Zavareze, L.-T. Lim, A.R.G. Dias, Development of antimicrobial and antioxidant electrospun soluble potato starch nanofibers loaded with carvacrol, Int. J. Biol. Macromol. 139 (2019) 1182–1190, https://doi.org/10.1016/j.ijbiomac.2019.08.096.

[13] Y. Liu, D. Wang, Z. Sun, F. Liu, L. Du, D. Wang, Preparation and characterization of gelatin/chitosan/3-phenylacetic acid food-packaging nanofiber antibacterial films by electrospinning, Int. J. Biol. Macromol. 169 (2021) 161–170, https://doi.org/10.1016/j.ijbiomac.2020.12.046.

[14] Y. Tang, Y. Zhou, X. Lan, D. Huang, T. Luo, J. Ji, Z. Mafang, X. Miao, H. Wang, W. Wang, Electrospun gelatin nanofibers encapsulated with peppermint and chamomile essential oils as potential edible packaging, J. Agric. Food Chem. 67 (8) (2019) 2227–2234, https://doi.org/10.1021/acs.jafc.8b06226.

[15] I. Kutzli, M. Gibis, S.K. Baier, J. Weiss, Electrospinning of whey and soy protein mixed with maltodextrin–influence of protein type and ratio on the production and morphology of fibers, Food Hydrocoll. 93 (2019) 206–214, https://doi.org/10.1016/j.foodhyd.2019.02.028.

[16] H. Li, S.-L. Chang, T.-R. Chang, Y. You, X.-D. Wang, L.-W. Wang, X.-F. Yuan, M.-H. Tan, P.-D. Wang, P.-W. Xu, Inclusion complexes of cannabidiol with β-cyclodextrin and its derivative: physicochemical properties, water solubility, and antioxidant activity, J. Mol. Liq. 334 (2021) 116070, https://doi.org/10.1016/j.molliq.2021.116070.

[17] H. Sadaquat, M. Akhtar, Comparative effects of β-cyclodextrin, HP-β-cyclodextrin and SBE 7-β-cyclodextrin on the solubility and dissolution of docetaxel via inclusion complexation, J. Incl. Phenom. Macrocycl. Chem. 96 (2020) 333–351, https://doi.org/10.1007/s10847-020-00977-0.

[18] Z. Liu, J. Zhang, P. Jiang, Z. Yin, Y. Liu, Y. Liu, X. Wang, L. Hu, Y. Xu, W. Liu, Paeoniflorin inhibits the macrophage-related rosacea-like inflammatory reaction through the suppressor of cytokine signaling 3-apoptosis signal-regulating kinase 1-p38 pathway, Medicine 100 (3) (2021), https://doi.org/10.1097/MD.0000000000023986.

[19] N. Khan, V.K. Bhardwaj, R. Purohit, A. Saneja, Deciphering the interactions of genistein with β-cyclodextrin derivatives through experimental and microsecond timescale umbrella sampling simulations, J. Mol. Liq. 374 (2023) 121295, https://doi.org/10.1016/j.molliq.2023.121295.

[20] D. Han, Z. Han, L. Liu, Y. Wang, S. Xin, H. Zhang, Z. Yu, Solubility enhancement of myricetin by inclusion complexation with heptakis-O-(2-hydroxypropyl)-β-cyclodextrin: a joint experimental and theoretical study, Int. J. Mol. Sci. 21 (3) (2020) 766, https://doi.org/10.3390/ijms21030766.

[21] A. Celebioglu, T. Uyar, Fast-dissolving antioxidant curcumin/cyclodextrin inclusion complex electrospun nanofibrous webs, Food Chem. 317 (2020) 126397, https://doi.org/10.1016/j.foodchem.2020.126397.

[22] L. Jiang, F. Jia, Y. Han, X. Meng, Y. Xiao, S. Bai, Development and characterization of zein edible films incorporated with catechin/β-cyclodextrin inclusion complex nanoparticles, Carbohydr. Polym. 261 (2021) 117877, https://doi.org/10.1016/j.carbpol.2021.117877.

[23] K. Pongsamart, W. Limwikrant, U.R. Ruktanonchai, N. Charoenthai, S. Puttipipatkhachorn, Preparation, characterization and antimalarial activity of dihydroartemisinin/β-cyclodextrin spray-dried powder, J. Drug Deliv. Sci. Technol. 73 (2022) 103434, https://doi.org/10.1016/j.jddst.2022.103434.
[24] E. Hsiung, A. Celebioglu, M.E. Kilic, E. Durgun, T. Uyar, Fast-disintegrating Nanofibrous web of pullulan/griseofulvin–cyclodextrin inclusion complexes, Mol. Pharm. 20 (5) (2023) 2624–2633, https://doi.org/10.1021/acs.molpharmaceut.3c00074.
[25] Z.-y. Qin, X.-W. Jia, Q. Liu, B.-h. Kong, H. Wang, Fast dissolving oral films for drug delivery prepared from chitosan/pullulan electrospinning nanofibers, Int. J. Biol. Macromol. 137 (2019) 224–231. https://doi.org/10.1016/j.ijbiomac.2019.06.224.
[26] T. Higuchi, K. Connors, Adv. Anal. Chem. Instrum, Phase-solubility techniques 4 (1965) 117–212.
[27] A. Celebioglu, T. Uyar, Encapsulation and stabilization of α-lipoic acid in cyclodextrin inclusion complex electrospun nanofibers: antioxidant and fast-dissolving α-lipoic acid/cyclodextrin nanofibrous webs, J. Agric. Food Chem. 67 (47) (2019) 13093–13107, https://doi.org/10.1021/acs.jafc.9b05580.
[28] C. Liu, R. Lu, M. Jia, X. Xiao, Y. Chen, P. Li, S. Zhang, Biological glue from only lipoic acid for scarless wound healing by anti-inflammation and TGF-β regulation, Chem. Mater. 35 (6) (2023) 2588–2599, https://doi.org/10.1021/acs.chemmater.3c00049.
[29] J.-Y. Park, T.-W. Chung, Y.-J. Jeong, C.-H. Kwak, S.-H. Ha, K.-M. Kwon, F. Abekura, S.-H. Cho, Y.-C. Lee, K.-T. Ha, Ascofuranone inhibits lipopolysaccharide–induced inflammatory response via NF-kappaB and AP-1, p-ERK, TNF-α, IL-6 and IL-1β in RAW 264.7 macrophages, PLoS One 12 (2) (2017) e0171322, https://doi.org/10.1371/journal.pone.0171322.
[30] J. Zhang, M. Zhang, X.-K. Huo, J. Ning, Z.-L. Yu, C. Morisseau, C.-P. Sun, B. D. Hammock, X.-C. Ma, Macrophage inactivation by small molecule wedelolactone via targeting sEH for the treatment of LPS-induced acute lung injury, ACS Cent. Sci. 9 (3) (2023) 440–456, https://doi.org/10.1021/acscentsci.2c01424.
[31] J.-W. He, P. Guo, L. Yang, J.-W. He, Anti-inflammatory constituents isolated from the flowers of Hosta plantaginea via suppression of the NF-κB signaling pathway in LPS-stimulated RAW 264.7 macrophages, RSC Adv. 13 (11) (2023) 7179–7184, https://doi.org/10.1039/D2RA07623C.
[32] M. Zhang, X. Wei, X. Xu, Z. Jin, J. Wang, Synthesis and characterization of water-soluble β-cyclodextrin polymers via thiol-maleimide 'click' chemistry, Eur. Polym. J. 128 (2020) 109603, https://doi.org/10.1016/j.eurpolymj.2020.109603.
[33] H. Maeda, T. Onodera, H. Nakayama, Inclusion complex of α-lipoic acid and modified cyclodextrins, J. Incl. Phenom. Macrocycl. Chem. 68 (2010) 201–206, https://doi.org/10.1007/s10847-010-9767-7.
[34] D. Poudel, S. Swilley-Sanchez, S. O'keefe, J. Matson, T. Long, C. Fernández-Fraguas, Novel electrospun pullulan fibers incorporating hydroxypropyl-β-cyclodextrin: morphology and relation with rheological properties, Polymers 12 (11) (2020) 2558, https://doi.org/10.3390/polym12112558.
[35] L. Wang, S. Li, P. Tang, J. Yan, K. Xu, H. Li, Characterization and evaluation of synthetic riluzole with β-cyclodextrin and 2, 6-di-O-methyl-β-cyclodextrin inclusion complexes, Carbohydr. Polym. 129 (2015) 9–16, https://doi.org/10.1016/j.carbpol.2015.04.046.
[36] M.R. de Freitas, L.A. Rolim, M.F.d.L.R. Soares, P.J. Rolim-Neto, M.M. de Albuquerque, J.L. Soares-Sobrinho, Inclusion complex of methyl-β-cyclodextrin and olanzapine as potential drug delivery system for schizophrenia, Carbohydr. Polym. 89(4) (2012) 1095–1100. https://doi.org/10.1016/j.carbpol.2012.03.072.
[37] Z. Qin, Y. Zou, Y. Zhang, P. Wang, H. Zhang, Electrospun pullulan nanofiber loading zanthoxylum bungeanum essential oil/β-cyclodextrin inclusion complexes for active packaging, Int. J. Biol. Macromol. 210 (2022) 465–474, https://doi.org/10.1016/j.ijbiomac.2022.04.155.
[38] G. Wang, Q. Zhan, H. Wu, Suppression of lipopolysaccharide-induced activation of RAW 264.7 macrophages by Se-methylseleno-l-cysteine, Int. Immunopharmacol. 89 (2020) 107040, https://doi.org/10.1016/j.intimp.2020.107040.
[39] Y. Nie, Z. Wang, G. Chai, Y. Xiong, B. Li, H. Zhang, R. Xin, X. Qian, Z. Tang, J. Wu, Dehydrocostus lactone suppresses LPS-induced acute lung injury and macrophage activation through NF-κB signaling pathway mediated by p38 MAPK and Akt, Molecules 24 (8) (2019) 1510, https://doi.org/10.3390/molecules24081510.
[40] C.H. Kim, B.S. Hwang, Y. Hwang, Y.T. Oh, J.-W. Jeong, Evaluation of antioxidant and antiinflammatory activity of ethanolic extracts of Polygonum senticosum in lipopolysaccharide-induced RAW 264.7 macrophages, JLM 46 (1) (2022) 51–59, https://doi.org/10.1515/labmed-2021-0099.
[41] M.-Y. Bai, Y.-M. Hu, Development of alpha-lipoic acid encapsulated chitosan monodispersed particles using an electrospray system: synthesis, characterisations and anti-inflammatory evaluations, J. Microencapsul. 31 (4) (2014) 373–381, https://doi.org/10.3109/02652048.2013.863395.
[42] A.K. Kiemer, C. Müller, A.M. Vollmar, Inhibition of LPS-induced nitric oxide and TNF-α production by α-lipoic acid in rat Kupffer cells and in RAW 264.7 murine macrophages, Immunol. Cell Biol. 80 (6) (2002) 550–557, https://doi.org/10.1046/j.1440-1711.2002.01124.x.
[43] V.G. DeMarco, P.O. Scumpia, J.P. Bosanquet, J.W., Skimming, α-lipoic acid inhibits endotoxin-stimulated expression of iNOS and nitric oxide independent of the heat shock response in RAW 264.7 cells, Free Radic. Res. 38 (7) (2004) 675–682, https://doi.org/10.1080/10715760410001702503.
[44] H.A. Aly, D.A. Lightfoot, H.A. El-Shemy, Modulatory role of lipoic acid on lipopolysaccharide-induced oxidative stress in adult rat Sertoli cells in vitro, Chem. Biol. Interact. 182 (2–3) (2009) 112–118, https://doi.org/10.1016/j.cbi.2009.08.013.
[45] I. Szulc-Kielbik, M. Kielbik, M. Klink, Ferulic acid but not alpha-lipoic acid effectively protects THP-1-derived macrophages from oxidant and pro-inflammatory response to LPS, Immunopharmacol. Immunotoxicol. 39 (6) (2017) 330–337, https://doi.org/10.1080/08923973.2017.1369100.
[46] X. Xia, C. Su, J. Fu, P. Zhang, X. Jiang, D. Xu, L. Hu, E. Song, Y. Song, Role of α-lipoic acid in LPS/d-GalN induced fulminant hepatic failure in mice: studies on oxidative stress, inflammation and apoptosis, Int. Immunopharmacol. 22 (2) (2014) 293–302, https://doi.org/10.1016/j.intimp.2014.07.008.
[47] Y. Wang, Y. Zheng, B. Qi, Y. Liu, X. Cheng, J. Feng, W. Gao, T. Li, α-Lipoic acid alleviates myocardial injury and induces M2b macrophage polarization after myocardial infarction via HMGB1/NF-kB signaling pathway, Int. Immunopharmacol. 121 (2023) 110435, https://doi.org/10.1016/j.intimp.2023.110435.
[48] H. Shi, X.-L. Wang, H.-F. Quan, L. Yan, X.-Y. Pei, R. Wang, X.-D. Peng, Effects of betaine on LPS-stimulated activation of microglial M1/M2 phenotypes by suppressing TLR4/NF-κB pathways in N9 cells, Molecules 24 (2) (2019) 367, https://doi.org/10.3390/molecules24020367.
[49] H. Xiong, Y. Cheng, X. Zhang, X. Zhang, Effects of taraxasterol on iNOS and COX-2 expression in LPS-induced RAW 264.7 macrophages, J. Ethnopharmacol. 155 (1) (2014) 753–757, https://doi.org/10.1016/j.jep.2014.06.023.
[50] P. Jing, Y. Luo, Y. Chen, J. Tan, C. Liao, S. Zhang, Aspirin-loaded cross-linked lipoic acid nanodrug prevents postoperative tumor recurrence by residual cancer cell killing and inflammatory microenvironment improvement, Bioconjug. Chem. 34 (2) (2023) 366–376, https://doi.org/10.1021/acs.bioconjchem.2c00548.
[51] D.-J. Kwon, S.M. Ju, G.S. Youn, S.Y. Choi, J. Park, Suppression of iNOS and COX-2 expression by flavokawain A via blockade of NF-κB and AP-1 activation in RAW 264.7 macrophages, Food Chem. Toxicol. 58 (2013) 479–486, https://doi.org/10.1016/j.fct.2013.05.031.
[52] Y. Ninomiya, S.-i. Tanuma, M. Tsukimoto, Differences in the effects of four TRPV1 channel antagonists on lipopolysaccharide-induced cytokine production and COX-2 expression in murine macrophages, Biochem. Biophys. Res. Commun. 484(3) (2017) 668–674. https://doi.org/10.1016/j.bbrc.2017.01.173.